Title

Biodistribution and toxicity of epitope-functionalized dextran iron oxide nanoparticles in a pregnant murine model

Journal

Journal of Biomedical Materials Research Part A, 108(5)

ISSN

1549-3296

Authors

Bolandparvaz, Amir

Vapniarsky, Natalia

Harriman, Rian

et al.

Publication Date

2020-05-01

DOI

10.1002/jbm.a.36893

Peer reviewed

HHS Public Access

Author manuscript

J Biomed Mater Res A. Author manuscript; available in PMC 2021 July 06.

Published in final edited form as:

J Biomed Mater Res A. 2020 May ; 108(5): 1186–1202. doi:10.1002/jbm.a.36893.

Biodistribution and toxicity of epitope-functionalized dextran iron oxide nanoparticles in a pregnant murine model

Amir Bolandparvaz[1], **Natalia Vapniarsky**[2], **Rian Harriman**[1], **Kenneth Alvarez**[1], **Jasmeen Saini**[1], **Zexi Zang**[1], **Judy Van De Water**[3,4], **Jamal S. Lewis**[1]

[1]Department of Biomedical Engineering, University of California Davis, Davis, California, USA

[2]Department of Pathology Microbiology and Immunology, University of California Davis, Davis, California, USA

[3]M.I.N.D. (Medical Investigation of Neurodevelopmental Disorders), University of California Davis, Davis, California, USA

[4]Department of Internal Medicine, Division of Rheumatology, Allergy, and Clinical Immunology, University of California Davis, Davis, California, USA

Abstract

In pursuit of a preventive therapeutic for maternal autoantibody-related (MAR) autism, we assessed the toxicity, biodistribution, and clearance of a MAR specific peptide-functionalized dextran iron oxide nanoparticle system in pregnant murine dams. We previously synthesized ~15 nm citrate-coated dextran iron oxide nanoparticles (DIONPs), surface-modified with polyethylene glycol and MAR peptides to produce systems for nanoparticle-based autoantibody reception and entrapments (SNAREs). First, we investigated their immunogenicity and MAR lactate dehydrogenase B antibody uptake in murine serum in vitro. To assess biodistribution and toxicity, as well as systemic effects, we performed in vivo clinical and post mortem pathological evaluations. We observed minimal production of inflammatory cytokines—interleukin 10 (IL-10) and IL-12 following in vitro exposure of macrophages to SNAREs. We established the maximum tolerated dose of SNAREs to be 150 mg/kg at which deposition of iron was evident in the liver and lungs by histology and magnetic resonance imaging but no concurrent evidence of liver toxicity or lung infarction was detected. Further, SNAREs exhibited slower clearance from the maternal blood in pregnant dams compared to DIONPs based on serum total iron concentration. These findings demonstrated that the SNAREs have a prolonged presence in the blood and are safe for

Correspondence: Jamal S. Lewis, University of California Davis, Department of Biomedical Engineering, 451 Health Sciences Dr. #3315, Davis, CA 95618. jamlewis@ucdavis.edu.

AUTHOR CONTRIBUTIONS

A.B. and N.V. contributed to the design and execution of experiments, analysis of data and compilation of the manuscript. R.H., K.A., J.S., and Z.Z. contributed to the execution of experiments and analysis of data. J.V. guided experimental design. J.S.L. contributed to the design of experiments, analysis of data, and manuscript compilation. J.S.L. has primary responsibility for the content of the manuscript.

CONFLICT OF INTEREST

All other authors have no conflict of interest to declare.

DISCLOSURE

Professor Van De Water has a patent application involving the MAR ASD peptides described herein.

SUPPORTING INFORMATION

Additional supporting information may be found online in the Supporting Information section at the end of this article.

use in pregnant mice as evidenced by no associated organ damage, failure, inflammation, and fetal mortality. Determination of the MTD dose sets the basis for future studies investigating the efficacy of our nanoparticle formulation in a MAR autism mouse model.

Keywords

clearance; distribution; histopathology; MAR autism; nanoformulation; peptide-functionalized

1 | INTRODUCTION

Autism spectrum disorder (ASD) comprises a range of neurodevelopmental disorders characterized by repetitive behaviors that significantly impair one's ability for social interaction (Williams White, Keonig, & Scahill, 2007). Currently, ASD is estimated to affect 1 in 59 children born in the United States (Baio et al., 2018). Although the etiology for ASD remains elusive, environmental and genetic factors may be at fault (Chaste & Leboyer, 2012). Furthermore, in approximately one quarter of ASD cases, maternal immune dysregulation results in production of autoantibodies to specific proteins, which react with the fetal brain (Meltzer & Van de Water, 2017). These specific proteins, including lactate dehydrogenase (LDH) B and Stress Induced Phosphoprotein 1 (STIP1), have been identified along with their dominant epitopic regions (Braunschweig et al., 2013). During gestation, maternal immunoglobulin G (IgG) antibodies cross the placenta into the fetal compartments to provide the IgG-naïve fetus with passive immunity (Garty, Ludomirsky, Danon, Peter, & Douglas, 1994). These antibodies maliciously react with fetal brain proteins and result in maternal autoantibody related (MAR) autism (Fox-Edmiston & Van de Water, 2015). Ostensibly, the removal of these pathological autoantibodies from maternal circulation may limit development of MAR autism in neonates (Fox-Edmiston & Van de Water, 2015). Seminal results from our previous publication demonstrated capture of MAR autoantibodies from human serum in vitro by MAR peptide-functionalized dextran iron oxide nanoparticles (DIONPs) (called SNAREs; [Systems for Nanoparticle-based Autoantibody Reception and Entrapment]; Bolandparvaz, Harriman, Alvarez, et al., 2019). This exciting nanoformulation development holds great promise for prevention of MAR autism and invites additional studies. Indeed, we recently reported formulation of ~15 nm MAR antigen-coated iron oxide nanoparticles (33.8 μg peptide/cm^2) with the ability to specifically capture high quantities of MAR autoantibodies from solution in vitro (Bolandparvaz et al., 2019). Remarkably, we demonstrated capture of 90% of LDH B autoantibodies in serum of mothers of children with autism (0.25 mg of SNAREs/ ml serum; Bolandparvaz et al., 2019). Prior to establishing the efficacy of the SNAREs in a pregnant C57BL/6j MAR autism mouse model (Judy Van de Water, Silverman, Yang, & Crawley, 2018), we must probe the maximum tolerated dose (MTD) in pregnant dams. We are at a critical transitional point to determine the safe use of iron oxide-based nanoparticulates in pregnant mice. In this vein, we interrogated SNARE toxicity, organ accumulation, and NP clearance in pregnant dams.

In the recent years, iron, gold, silver, and zinc, as well as other materials have proven constructive in the design of nanoparticulate therapeutics (Vinay Kumar & Maitra, 2017). For instance, iron oxide nanoparticles (IONPs) demonstrated desirable characteristics such

as high surface area to volume ratio, inherent magnetism, stability, bio-compatibility, cost-effectiveness, and eco-friendliness (Lu, Salabas, & Schuth, 2007; Stephen, Kievit, & Zhang, 2011). Owing to such properties, IONPs are now either commercially available or under research scrutiny for various biomedical applications, such as magnetic resonance imaging (MRI) contrast (Lu, Cohen, Rieves, & Pazdur, 2010), gene delivery (Kami et al., 2011), hyperthermia-based cancer treatments (Banobre-Lopez, Teijeiro, & Rivas, 2013), and removal of environmental contaminants (Wu, Wu, Yu, Jiang, & Kim, 2015). Notably, IONPs are approved by the Food and Drug Administration (FDA) for use as iron deficiency supplements (Feraheme) and MRI contrast agents (Feridex) (Lu et al., 2010). Despite these favorable characteristics, there exists a major gap in translation of IONP-based products into the clinic due to potential toxicity. Yet, the tremendous therapeutic potential of IONP nanoformulations demands further study of toxicity and establishment of their biosafety (Wang, 2015). In this realm, we seek to legitimize the use of an iron oxide-based nanoparticle system in pregnant mammals.

Only a handful of studies have investigated the biological effects and toxicity of IONP (Feng et al., 2018; Singh et al., 2006; Unterweger et al., 2017) and a few publications probed the effects of IONP in the fetal compartment (Ali Noori, Modaresi, Messripour, Yousefi, & Amiri, 2011; Di Bona, Xu, Gray, et al., 2015). Seemingly, the results on biodistribution, toxicity, and clearance of IONPs reported in literature are divergent, due to the variations in size, surface-coating (e.g., dextran, polyethylene glycol (PEG), citric acid), surface-charge, and experimental conditions (e.g., route of administration, cell types, incubation time points; Feng et al., 2018). Amid such concerns, the next major step is to establish the safety of our SNARE formulation in pregnant mice, which will serve as the test bed for future efficacy studies should safety worries be set aside.

The objective of this study is to investigate acute and sub-chronic toxicity of the SNAREs in a pregnant murine model. These SNAREs are under investigation as scavengers of malicious autoantibodies circulating in the maternal blood. Here, we aim to describe and report on potential adverse effects associated with intravenous (I.V.) administration of SNAREs in healthy pregnant mice. Moreover, this study will be deterministic of the appropriate dose for this nanoparticle prophylactic in future studies to evaluate its therapeutic efficacy.

2 | MATERIAL AND METHODS

2.1 | Nanoparticle synthesis

We synthesized ~15 nm dextran DIONPs similar to Jarret et al. coprecipitation method (Jarrett, Frendo, Vogan, & Louie, 2007) with the modification of adding nonreduced dextran (*Leuconostoc mesenteroides*; average MW: 9,000–11,000; Sigma Aldrich, St. Louis, MO). We physico-chemically characterized the DIONPs using dynamic light scattering (DLS) and transmission electron microscopy (TEM). Next, DIONPs were surface-decorated with citric acid (CA) (Sigma Aldrich) to add carboxyl groups on the surface for further modification. Further, we added Methoxy PEG amine (10 kDa) (PolySciences, Warrington, PA) at 10:1 ratio (% w/w) to amine reactive DIO-CA NPs via carbodiimide chemistry. The zeta potential measurements were acquired using Malvern ZetaSizer Nano ZS (Malvern Instruments, Malvern, UK) (Bolandparvaz et al., 2019).

2.2 | Generation of bone marrow-derived macrophages

Macrophages were extracted from 8 to 12 weeks old male and female C57BL/6j mice (Jackson Laboratories, Bar Harbor, ME) in accordance with the UC Davis Institutional Animal Care and Use Committee (IACUC) guidelines and a modified 10-day protocol (Lewis et al., 2013; Riley, Allen, Jeffrey, Manickam, & Lewis Latent, 2018). To obtain the cells, mice were euthanized by CO_2 inhalation followed by cervical dislocation and the femurs and tibia of the mice were harvested by surgical intervention. The cells of the bone marrow were flushed out of the bone using a 25-gauge needle and a 10 ml syringe filled with wash buffer (RPMI medium with L-glutamine, 25 mM HEPES (Mediatech, Manassas, VA), 1% FBS (Mediatech) and 1% penicillin–streptomycin (Hyclone, Logan, UT)). The bone marrow cell suspension was strained using a 70 μm cell strainer (Becton Dickinson, Franklin Lakes, NJ) to remove bone and tissue impurities. The subsequent suspension was spun at 1,800 rpm (305 g) for 5 min to pellet cells. To lyse the red blood cells (RBCs), 3 ml of ACK lysis buffer (Lonza, Walkersville, MD) was added and incubated for 3 min followed another step of centrifugation at 1,800 rpm (305 g) for 5 min. Leukocytes were suspended in media consisting of DMEM/F-12 1:1 with L-glutamine (Cellgro, Herndon, VA), 10% FBS, 1% penicillin/streptomycin (Hyclone), 1% sodium pyruvate (Lonza), 20 ng/ml Macrophage-Colony Stimulating Factor (M-CSF) (R&D systems, Minneapolis, MN), and seeded in a tissue culture flask for 6 days. Subsequently, cells were lifted by incubating with 2 mM Na_2EDTA (Thermo Fisher Scientific, Waltham, MA) in a PBS solution at 37°C for 10 min and resuspended in cell culture media. The cells were then transferred to tissue culture plates and allowed for macrophage adhesion and proliferation. On Day 10, cells were utilized for studies.

2.3 | Cytokine release by macrophages

Bone-marrow derived macrophages were seeded in 12 well plates and treated with SNAREs and DIONPS at 100 μg/ml concentration on Day 10 of cell culture. This NP concentration was previously used to assess the effect of iron oxide NPs on macrophage maturation (Rojas et al., 2016). Control groups were designated as immature macrophages (iMacs) as negative control and lipopolysaccharide-(LPS; 1.5 μg/ml, Sigma Aldrich) treated cells as positive control. Cells were incubated at 37°C and 5% CO_2 for a period of 24 and 48 hr prior to analysis. Cell supernatants were collected and used to immediately perform IL-12 and IL-10 ELISAs (BD Bioscience, San Jose, CA, USA), following the manufacturer protocols.

2.4 | Animal care and mating

Animal work was performed under strict UC Davis IACUC guidelines. Eight-weeks-old male and female C57BL/6j mice (Jackson Laboratories, Bar Harbor, ME) were housed at the UC Davis Genome and Biomedical Sciences Facility Vivarium. For all in vivo studies, one or two female mice ($N = 70$) were caged with one male mouse ($N = 35$) in separate cages and pregnancy of the dams was confirmed the following days with the observation of a copulation plug (gestational day [GD] 0) and tracking the weight gain. Dams were separated and randomly assigned to treatment groups after confirmation of pregnancy and uniquely identified using a tail color-marking scheme. Male mice were euthanized via CO_2 inhalation and cervical dislocation at the end of the mating period. For in vitro antibody capture studies

in mouse serum, UCD Comparative Pathology Lab immunized 4 male mice (C57BL/6j) (Charles River Laboratories, Wilmington, MA), ~9 weeks old and housed the mice at the UC Davis MS1/Tupper Hall Vivarium.

2.5 | In vitro capture of MAR autoantibodies in mouse serum

Mice (C57BL/6j) were immunized with LDH B peptide (amino acid sequence: PVAEEEATVPNNKIT; Genscript, Piscataway, NJ) via intra-peritoneal (I.P.) injection and serum collected at 2 week intervals up to 8 weeks postinjection. In an antibody titer assay, serial dilutions of the serum were made by diluting in PBS at ratios of 1:250, 1:1,000, 1:10,000, and 1:100,000. Serum samples diluted 1:250 were mixed with 0.01, 0.05, and 0.25 mg/ml of SNAREs, DIONPs, and DIONPs conjugated to scrambled peptide (EIPAENVTEVTPNKA) overnight at 37°C and magnetically separated. Following incubation, NPs were separated from the solution via a magnetic column and centrifugation. An indirect enzyme-linked immunosorbent (ELISA) assay was performed on the supernatant. A 2 μg/ml biotin-LDH B peptide-coating buffer solution was left in a 96 well ELISA plate (Corning Costar, Corning, NY) at 4°C overnight. Subsequent steps included-washing five times with 0.05% Tween-20 (Sigma Aldrich), and blocking with 2% normal goat serum (NGS; Thermo Fisher Scientific) in PBS suspension for 1 hr at 37°C. Following five 0.05% Tween-20 washes, 50 μl of supernatants and standards were half-diluted with 50 μl of 4% NGS in PBS then incubated for an additional hour. The plate was again washed and secondary alkaline phosphatase-conjugated antibody (Thermo Fisher Scientific) was diluted (1:10,000) in blocking buffer. Following a 1 hr incubation period at 37°C, the plate was washed five times with 0.05% Tween-20. Briefly, a 4-methylumbelliferyl phosphate (4-MUP; Sigma Aldrich) substrate solution (2.5 mg/ml) was added and fluorescent reading (ex/em: 386/448 nm) taken after 1 hr at 37°C. A standard curve was obtained from the serial dilutions and used to calculate corresponding sample titer. Additionally, isotype control antibodies lacking specificity for the LDH B peptide was used as a negative control.

2.6 | MTD in vivo

In this study, the MTD dose is defined as the highest tolerated dose with no major life-threatening toxicity (Zhang, Zeng, & Lu, 2015). Dosage range of SNAREs was established based on our in vitro viability results which showed that the 25% lethal concentration (LC25) was ~500 μg/ml (Kermanizadeh et al., 2013). Given the average blood volume of a 25 g C57BL/6j mouse is ~1.46 ml of blood, we extrapolated a dose of 0.73 mg of SNAREs/NPs would correlate to the determined in vitro LC25 (NC3Rs, n.d.). The NPs were injected on GD 12, when placental receptors for transplacental movement of MAR Abs appear. Procedurally, mice were briefly sedated through isoflurane (Thermo Fisher Scientific) inhalation and placed in tail injector restrainer for I.V. NP injection via a catheter. Treatments groups ($n \geq 6$; 200 μl PBS) were: 1. control group (phosphate-buffered saline [PBS] only; 2. DIONPs (30 mg NPs/kg equivalent of 1 × LC25); 3. SNAREs (3 mg NPs/kg equivalent of 0.1 × LC25); 4. SNAREs (15 mg NPs/kg equivalent of 0.5 × LC25); 5. SNAREs (30 mg NPs/kg equivalent of 1 × LC25); 6. SNAREs (150 mg NPs/kg 5 × LC25; two injections of 200 μl each in PBS were administered 30 min apart); 7. SNAREs (300 mg NPs/kg equivalent of 10 × LC25 (two injections as in group 6). On a daily basis, dams were monitored for signs of morbidity, such as sudden weight loss, changes in behavior, breathing

rate, food consumption, and impairment in motility. Dams were euthanized by CO_2 inhalation and cervical dislocated if humane endpoints, such as sudden weight loss (20%), inability to consume food (i.e., lethargy, hunched posture, inability to rise), altered respiratory rate, and rough hair coat, manifested. Notably, the health of the mother is in direct correlation with fetal health, and materno-toxicity could translate into harmful effects on the fetus (Chernoff, Rogers, Gage, & Francis, 2008). As such, dams were euthanized prior to parturition at GD 17 if humane endpoints were not reached. If dams gave birth earlier, the litters were euthanized via intra-peritoneal administration of Euthasol and decapitation.

2.7 | Hematological and chemical assessments of peripheral blood

Serum was assessed for iron concentration and biochemical composition. Serum iron concentration was assessed using an iron assay kit (Roche, Basel, Switzerland). Likewise, serum samples were submitted for analyses of creatinine and blood urea nitrogen (BUN; i.e., kidney function; Bungener et al., 2002), alanine aminotransferase (ALT) and bilirubin (i.e., liver function) (Cobas Integra, Basel, Switzerland; Gu, Fang, Sailor, & Park, 2012) at the UC Davis Clinical Pathology Laboratory. Heparinized whole blood was analyzed for hemoglobin concentration, and white and red blood cell counts using a Beckman Coulter AC-T Hematology Analyzer.

2.8 | Necropsy and Histopathological analysis

Immediately upon sacrifice, blood was collected via cardiac puncture into heparin-coated microtubes and yellow-capped microtainer gel separator tubes for hematological and serological assessment (Becton Dickinson, Franklin Lakes, NJ). Following blood collection, full necropsy was performed, which included gross evaluation of all body systems, weighing of uteri, spleen, liver, kidneys, lungs, and heart, documentation of fetal number and condition, and collection of samples for histological analysis. Maternal weight gain (MGW) was determined by subtracting the combined weight of the dam at GD 0 and uteri from the weight of the dam at GD 17. Frequency of fetal resorption was determined based on the number of resorption/total number of fetuses compared to control mice. Representative samples of cardiovascular, musculoskeletal, digestive, urogenital, cutaneous, nervous, and lymphatic systems were collected and fixed in 10% neutral buffered formalin. Fixed tissues were then processed for routine histology and stained with hematoxylin eosin and Prussian Blue iron stain. The histological analysis and grading were performed by a board certified veterinary anatomic pathologist (NV).

2.9 | Biodistribution via Prussian blue analysis

To observe presence of iron in various tissues, Prussian Blue staining with a nuclear fast red counterstain (Sigma-Aldrich, St. Louis, MO, USA) was performed on formalin fixed paraffin embedded sections of major organs according to an established protocol (Carson, 2009). Stained sections were imaged in their entirety with a Keyence BZ-X700 microscope (Keyence, Osaka, Japan) at ×20 magnification, in brightfield with a full color filter. At least six organs of same type per each group of mice were quantified with the ImageJ (Fiji) software.

2.10 | Biodistribution and clearance via MRI

Once the MTD dose was determined at 150 mg NPs/kg, another cohort of pregnant dams was injected with SNAREs and DIONPs at 100 mg NPs/kg and SNAREs at 30 mg NPs/kg. These doses were chosen to serve as a starting point based on our MTD studies as well as other reports (Cook, Hansen, Siu, & Abdul Razak, 2015). The NP formulations were administered intravenously on GD 12 at previously mentioned doses—30 and 100 mg NPs/kg. Alternatively, pregnant mice in the control group received 200 μl of saline. The mice receiving SNAREs were then subjected to MRI screening at 4, 24, and 120 hr. MRI was captured at 4, 24 hr, and 5 days post administration ($n \geq 3$) using a 35 mm coil with a pulse sequence on a Bruker Biospec 70/30 (Bruker, Billerica, MA) at the UC Davis Center for Molecular and Genomic Imaging (CMGI) and images analyzed using Slicer and ImageJ. Additionally, blood samples were obtained from tail vein in the groups receiving 100 mg NPs/kg SNAREs and DIONPs at 30 min, 1, 2, 4, 8, and 24 hr for serum iron concertation assessment. The clearance rate of SNAREs was assessed via measurement of total serum iron concentration on blood samples collected from tail vein at 30 min, 1, 2, 4, 8, 24 hr time points for the 100 mg NPs/kg dose. The area under the curve (AUC) was calculated using Prism (Version 8) following linear plotting of the data.

2.11 | Statistical analysis

Data was analyzed using one-way or two-way analysis of variances (ANOVA) followed by posthoc Tukey comparison test using the mean of each treatment group in Prism (Version 8). Where relevant, data are presented as the mean ± standard error (Ghasempour, Shokrgozar, Ghasempour, & Alipour, 2015). Mean of every treatment was compared to the control and significance was determine and denoted by (*) for $p < .05$, (**) for $p < .01$, (***) for $p < .001$, and for $p < .0001$. We used at least three biological replicates and three technical replicates for the in vitro studies. For mouse safety studies, each treatment group included at least six pregnant dams and for MRI studies, we used at least four pregnant dams per treatment group.

3 | RESULTS

3.1 | Nanoparticle synthesis and characterization

The DIONPs and SNAREs demonstrated uniform dispersity in DI H_2O (Figure 1a,b). TEM and DLS analysis of the DIONPs demonstrated uniform particle shape and size of ~15 nm (average hydrodynamic diameter) (Figure 1c,d). Zeta potential measured at physiological pH was −7.4 mV for DIONPs and −20.36 mV for SNAREs (Figure 1e). Further, we quantified a peptide surface density of 33.8 μg peptide/cm^2 (Bolandparvaz et al., 2019).

3.2 | Cytokine release by macrophages

We assessed immunogenicity of SNAREs and naked DIONPs on bone-marrow derived macrophages at 24 and 48 hr. Specifically, the secretion of IL-10 and IL-12 cytokines in presence of DIONPs and SNAREs was also quantified. iMacs (untreated, immature macrophages) as well as lipopolysaccharide (LPS)-treated macrophages were used as the negative and positive controls, respectively. In comparison to LPS-treated macrophages,

IL-10 and IL-12 secretion were significantly diminished in the presence of SNAREs and DIONPs at both time points (Figure 2).

3.3 | Assessment of MAR LDH B autoantibody capture in vitro

In vitro, we demonstrated ~87% reduction of MAR LDH B antibody titer in mouse serum treated with SNAREs (0.25 mg/ml; Figure 3). Moreover, isotype controls as well as standard antibody titer dilutions were used to qualify the results (Figure S1). Further, a scrambled version of the LDH epitope of SNAREs and plain DIONPs were used as negative controls and exhibited minimal antibody reduction capability.

3.4 | MTD in vivo

Critical for the translation of our SNARE formulation, we investigated the MTD in C57BL/6j pregnant dams. To determine the MTD dose, we assessed the maternal mortality, body weight, clinical signs (e.g., acute pain or distress), food consumption, hematology, and serum chemical composition. Further, we grossly examined all major organs at the terminal time point and performed histopathological assessments. Acute mortality was observed in mice treated with 300 mg NPs/kg SNARE dose (N = 3/4 mortality immediately after injection). Mice injected with this dose exhibited immediate discomfort represented by a rapid breathing. As mice were disassociated from isoflurane sedation, there was no movement, or a heartbeat and mice were reported deceased. On the other hand, the dose of 150 mg NPs/kg was well tolerated as evident by no difficulty in breathing, absence of acute pain or distress, normal walking, grooming, and food consumption. Likewise, total maternal weight progressively increased in all treatment groups from GD 0 to GD 12, validating pregnancy. Maternal weight continued to increase following NP injection and was not significantly different from the saline control group (Figure 4a). No significant difference was observed in MGW (weight of dam at GD 17 − [weight of dam at GD 0 + weight of uteri]) between any of the treatment groups and control group (Figure 4b, Table S1). We observed no significant difference amongst the treatment groups and control in frequency of fetal resorption (Figure 4c, Table S2) in dams treated with SNAREs. Moreover, we detected no difference in the fetal size or litter size among the treatment groups and control and no developmental anomalies were observed in the fetuses. Histologically, fetal tissues had no iron accumulation—even mice that received higher doses of SNAREs. Collectively, these findings indicate an absence of fetal toxicity (Di Bona et al., 2015) and suggest that the MTD of the SNAREs is around 150 mg NPs/kg.

3.5 | Hematological and chemical assessments of peripheral blood

Full necropsy was performed on GD 17. No abnormalities were detected grossly except in one mouse that received dose of 150 mg NPs/kg, in which liver was diffusely darker than in the other mice. This color change was not associated with histological abnormalities and was attributed to post mortem blood pooling. Creatinine, blood urea nitrogen, ALT, and bilirubin values showed no significant deviation from normal range values in any of the treated groups and no significant difference was found from saline-treated control group and DIONP-treated dams (Figure 5, Table S3). Hematological analysis showed no alteration from normal range values in white blood cell (WBC) count, red blood cell (RBC) count, or hemoglobin concentration amongst the treatment groups and no significant difference was found in these

values when compared to saline control and DIONP-treated mice (Figure 6, Table S4). Further, weight of maternal uteri, liver, kidneys, and spleen (Figure 7, Table S5) was similar for all groups.

3.6 | Necropsy and Histopathological analysis

The summary of histological analysis are presented by treatment groups below (Figures 8 and 9, Figures S2–S3, Table S6):

1. DIONP (30 mg NPs/kg); In the lung, brown, homogeneous, round to oval aggregates, ranging in size from 2.5 to 7.5 μm in diameter, were present within the lumina of small capillaries. The occurrence of these particles in the pulmonary tissues of animals in this group was rare and no pathologic changes such as infarction or inflammation were associated with their presence in the tissue. In the liver, the brown black pigment accumulation was observed in the Kupffer cells. The frequency of cells that accumulated this pigment was low and Kupffer cell size was not increased due to pigment accumulation. Besides minimal rare areas of acute hepatocellular necrosis associated with mixed leukocyte infiltration in two out of eight livers, no other pathological changes were observed in the liver sections (Figure S3a). The areas of necrosis were not associated with iron pigment and were sub-acute. Rare brown aggregates identical to those described in the lung were present within the capillaries of the glomerular tufts in the kidney sections in one animal. As with other organs, no pathological changes or inflammation were appreciated in the renal tissue. In the spleen, physiological accumulation of the yellow pigment-laden macrophages was observed in the red pulp. The pigment is likely represents normal iron deposits characteristic to this organ. No pathologic changes and no pigment accumulation were appreciated in the sections of the heart, pancreas, placenta, or within any of the fetal tissues.

2. SNARE (3 mg NPs/kg); Minimal to no abnormalities were detected in the tissues of animals in this group. Occasional smooth, oval to round, homogeneously brown material deposits, measuring 2–4 μm in diameter, were observed in the lumina of the pulmonary capillaries. No tissue infarction or inflammation was associated with these particles. Small amount of yellow intracytoplasmic pigment was detected in the red pulp macrophages in the spleen, which was considered normal physiological site of iron accumulation as the amount of splenic macrophage pigment in this group was not different from control group. In one animal, liver contained rare foci of acute hepatocellular necrosis associated with pleocellular leukocyte infiltration (Figure S3a). Provided similar foci of individual hepatocellual necrosis were observed in the saline control groups (Figure S3d) and no clinical findings associated with liver disfunction were detected, these findings were considered incidental.

3. SNARE (15 mg NPs/kg); Minimal to no abnormalities were detected in the examined tissues. In the liver sections, rare round to oval, homogeneously brown material was rarely detected within the sinusoids and occasional Kupffer cells. Similar material was infrequently observed in the lumina of the pulmonary

capillaries. Physiological quantities of intracytoplasmic yellow pigment were present in red pulp macrophages in the spleen. One animal has evidence of minimal *Pneumocystis murina* yeast infection in the lung, which was classified an incidental finding (Figure S3b).

4. SNARE (30 mg NPs/kg); In the liver sections, pigments were present in the occasional Kupffer cells with no apparent effect on the hepatocytes. The pulmonary capillaries occasionally contained round brown homogeneous material. In the kidney, the lumina of rare glomerular capillaries were occluded by similar material. There was no evidence of infarction or cellular degeneration in any of the organs that contained pigment. Rare cases have slightly more than physiological level accumulation of pigment-laden macrophages in the red pulp of the spleen. No pigment was observed in the placenta or fetal tissues and no inflammation was appreciated in any of the examined organs (Figure 8, Grade 0).

5. SNARE (150 mg NPs/kg); Lung was the tissue with maximal amount of intravascular brown homogeneous material. The presence of this material in the lung was associated with mild degree of congestion of the pulmonary vasculature (Figure 8, Grade III). In the liver, pigmented material was primarily observed within the Kupffer cells at moderate to high frequency (Figure 8, Grade III). Red pulp macrophages in the spleen contained large amounts of pigment that was above physiological normals (based on saline controls; Figure 8, Grades II and III). In the kidney, the brown pigment was present within glomerular capillaries and occasionally in the renal venules. In the heart, the particles were observed in the ventricles (Figure S3c) and occasionally within small coronary capillaries (Figure 8). Despite increased frequency and quantity of the pigmented material in the organs mentioned above, there was no evidence of parenchymal damage, infarction or inflammation. In one animal the brown particulates were observed in the placental blood vessels. However, there was no evidence of particulate material in the fetal tissues (Figure 8, Grade III).

6. In the animals that received a dose of 300 mg NPs/kg that lead to major fatality, brown particulates were abundant within pulmonary vasculature. The presence of these particulates was associated with severe pulmonary conjestion. Additionally, heart ventricles were extended with blood, suggesting circulatory failure as ventricles did not pump out the blood. Given the evidence for pulmonary vasculature tree and cardiac congestion accompanied with complete absence of particulate material in the vasculature of any other organs, cause of death was determined to be acute circulatory failure.

In summary, these findings suggest that 150 mg NPs/kg was the highest tolerated dose. It was concluded that this dose was safe in this short-term safety study as there were no overt signs of toxicity or mortality as minimal tissue damage or inflammation was detected in any of the organ systems examined.

3.7 | Biodistribution via Prussian blue analysis

Prussain Blue and Nuclear Red counterstain of histological slides demonstrated a progressive increase in iron content in liver, lung, heart, spleen, and kidney with an increase in the SNAREs dosage. Further, Prussian Blue histochemical anlaysis revealed iron positive material intravascularly in the organs mentioned above. A significantly higher iron concetration was detected in the liver and lungs of mice treated with SNARE dose of 150 mg NPs/kg at 3.37 ± 1.34% and 6.40 ± 1.13% of the total organ area respectively compared to the saline-treated control at less than 1% (Figures 10–12, Figure S4, Table S7). Further, we observed no accumulation in the fetuses relative to the saline control at 30 mg NPs/kg and no significant increase in iron content at 150 mg NPs/kg. Overall, there was a general trend of marginal increase of iron content in all the tested organs at the 150 mg NPs/kg.

3.8 | Biodistribution and clearance via MRI

Biodistribution of SNAREs were assessed via MRI at 30 and 100 mg NPs/kg, slighlty lower doses than the MTD (150 mg NPs/kg). Dosage testing in clinical translation often starts with a lower dose and is progressively increased up to the MTD (Cook et al., 2015). The maternal liver demonstrated significant accumulation of both doses of SNAREs by 4 hr and persisted at 5 days postinjection (Figure 13, Figure S5). Further, the maternal kidneys exhibited significant accumulation of SNAREs at the 100 mg NPs/kg by 4 hr and up to the 24 hr examined. The large size and number of fetuses at GD 17 (5 days postinjection) eclipsed the kidneys and we were not able to measure the iron accumulation in the kidneys via MRI on Day 5. Further, we could not assess deposition of iron in the lungs using this method, due to susceptibility artifacts at the air-tissue interface and low proton density in the lungs interfering with the MRI imaging (Biederer et al., 2012). Notably, fetuses exhibited no detectable accumulation of NPs.

Dams administered SNAREs demonstrated slower clerance of iron compared to DIONP-injected dams at time points earlier than 8 hr postinjection (Figure 14a). By 24 hr, the blood total iron concentration for saline-treated controls were comparable to nanoparticle-injected mice, indicating clearance from the circulation. AUC confirmed the slightly slower clearance of SNAREs with AUC of 3,518 ± 260 μg hr/dl compared to DIONP AUC of 3,147 ± 420 μg hr/dl and saline AUC of 2,833 ± 260 μg hr/dl (Figure 14b).

4 | DISCUSSION

The primary objectives of this study were to determine the highest tolerated dose of SNAREs, assess their biodistribution and clearance, as well as evaluate their organ toxicity. We determined that 150 mg NPs/kg is the highest tolerable dose as we observed no signs of overt toxicity or mortality. Further, we observed minimal evidence of inflammation locally or systemically in the animals that received this dose. Importantly, we were able to predict, with fair accuracy, the biologically relevant dose of the formulation based on in vitro toxicity assessments. We also demonstrated that SNAREs clear the blood circulation within 24 hr of intravenous administration. Collectively, these findings pave the way for further development of a MAR autism prophylactic nanoformulation and warrant more preclinical studies to advance this prophylactic.

One of the first barrier nanoparticles face after intravenous administration is phagocytosis by the antigen presenting cells (APCs; i.e., DCs and macrophages), which could lead to the activation of these innate immune cells. For our application, it is imperative that SNAREs limit interaction with immune cells and minimize their activation. Thus, we evaluated if therapeutic application of SNAREs is associated with APC activation. Previously, we demonstrated SNAREs co-incubated with DCs or macrophages for 24 and 48 hr did not induce maturation (Bolandparvaz et al., 2019). This finding is seminal to our SNARE formulation to evade an immune response and prevent generation of antibodies, as reported with adjuvant-coated NPs (Neto, de Sousa-Júnior, da Costa, & Kipnis, 2018). Here, we examined the production of IL-10 and IL-12 as these are the primary cytokines produced by activated APCs (Ma, Yan, Zheng, et al., 2015). We observed no significant change in IL-10 or IL-12 production in bone marrow-derived macrophages treated with SNAREs or DIONPs. Previously, we demonstrated a significant increase in pro-inflammatory IL-12 production by bone marrow-derived DCs in presence of DIONPs but not SNAREs (Bolandparvaz et al., 2019). Such disparity in DC versus macrophage release of IL-12 in presence of DIONPs may be due to their use of different TLRs for IL-12 production (Pompei et al., 2007). This lack of cytokine secretion, particularly inflammatory cytokines, has implications downstream due to interactions with adaptive immune cells. Succinctly, activation and polarization of naïve T cells into Th1 cells is less likely without the IL-12 (Athie-Morales, Smits, Cantrell, & Hilkens, 2004). It should be noted that other inflammatory cytokines that play a role in T cell activation were not investigated. However, given on previous results on surface makers, there is enough evidence that the SNAREs are not immunogenic. This characteristic is likely due to the dextran and PEG coating, as previously suggested by others (Feng et al., 2018; Unterweger et al., 2017).

Advancing the development of a nanoparticulate therapeutic for MAR autism, we evaluated capacity of SNAREs to trap MAR LDH B antibody from mouse serum. Consistent with our previous findings demonstrating capture of up to 90% from MAR autism patient-derived serum, we showed removal of up to 87% of LDH B antibodies in vitro from diluted mouse serum using 0.25 mg/ml of SNAREs. Further, we established increased entrapment of LDH B antibodies with increased concentration of SNAREs. These findings demonstrate the ability of SNAREs to specifically target MAR antibodies from a mixture of antibodies. In a similar realm, Hu et al. reported on red blood cell membrane-derived biomimetic NPs conjugated with poly(lactic-co-glycolic) acid (PLGA) NPs serving as a sponge to capture malicious antibodies associated with type II hypersensitivity reaction. Collectively, our promising in vitro results stimulated execution of safety studies (Hu et al., 2011).

In this vein, we investigated the MTD, biodistribution, and clearance of SNAREs in pregnant dams. Clinical follow up of the dams during the study showed progressive weight gain across the treatment groups. Further, although serum biochemical parameters were measured 5 days following NP injection, we do not consider this a limitation. Despite a short half-life of these metabolites (in the order of a few hours; Chiou & Hsu, 1975), high concentrations, in the event of severe organ cellular damage, persists for at least several days (Gowda et al., 2009) and would be accompanied by obvious histological changes which we did not observe. Due to the potential immunogenicity of these peptide-functionalized IONPs and accelerated RBC production from excess iron, we investigated the levels of white and red

blood cells, along with hemoglobin. We observed no significant change in these hematological parameters. Further, our results fell within the permittable range based on references from nonpregnant 2–3 months old male C57BL/6j mice for hematological studies (Santos et al., 2016).

The gross postmortem evaluation of the animals revealed no signs of organ enlargement, inflammation, or failure. Quantitative assessment of the essential organs' weights relative to whole body weight revealed no differences between treatment groups and controls, further supporting no change in the size of the organs. Extensive histopathological evaluation of SNARE-treated mice supported the hypothesis that this formulation would be safe at therapeutic concentrations. Expectedly, the IONPs were phagocytosed by cell of reticuloendothelial system as evidenced by accumulation of brown pigment in the Kupffer cells in the liver and red pulp macrophages in the spleen. Prussian Blue (iron histochemical staining of the organs) confirmed the iron nature of the pigment. The quantitative assessment of the iron in major organs revealed significant differences in the content of this compound only in the lung and liver and there was a proportional increase in iron concentration relative to the dose. Interestingly, in the lung and at the highest administered dose, there was brown material present within and occluding the lumens of small capillaries rather than within phagocytic cells. The size of the smallest pulmonary capillary in murine species is <25 μm (Townsley, 2012). This diameter is much larger than the diameter of the injected IONPs which indicates that the occlusion of the capillaries was made by aggregates of the IONPs. Due to dual blood supply of the pulmonary tree, such occlusion did not lead to infarction of the lung, nor was there evidence of inflammation associated with the embolized particles. It remains to be determined if partial/complete occlusion of the pulmonary capillaries will eventually result in phagocytic clearance of the embolized material and if retention of the aggregated IONPs in the pulmonary circulation can offer prolonged capturability of MAR autoantibodies.

Assessment of the distribution and clearance of SNAREs with Prussian Blue iron stain and MRI echoed the histopathological observations. We demonstrated significant deposition of iron in the liver and the lungs of mice treated at 150 mg NPs/kg SNARE formulation. The accumulation of the nanoparticles in the lungs was not surprising as the pulmonary capillary bed is the first capillary network particles encounter upon tail-vein injection (Townsley, 2012). Further, the presence of the SNAREs in the capillary beds of the liver and kidney indicate their extensive distribution. This finding is important because similar formulations can be employed for targeted delivery and treatment of other disease entities in these organs. These observations are in agreement with other reported results demonstrating significant accumulation in the lungs and liver for intravenously injected NPs (Park et al., 2016; Sharma et al., 2018). For example, Sharma et al injected citrate-stabilized IONP surface-coated with negatively charged carboxymethyl dextran (CM) or positively charged PEG-Polyethyleneimine (PEI) at a dose of 8 mg NPs/kg into retro-orbital plexus of male athymic nude mice. The CM-modified CA-IONPs demonstrated highest deposition in spleen and liver, while PEG-PEI CA-IONPs were deposited mainly in the lungs (Sharma et al., 2018). Further, PEG-PEI CA-IONPs appeared to be localized within lung epithelial cells, whilst CM-coated CA-IONPs were localized in the interstitial spaces, ostensibly due to surface charge differences. Additionally, Sharma et al reported blood iron content similar to controls

at 24 hr, suggesting clearance of nanoparticles from blood circulation. In summary, biodistribution of SNAREs (and DIONPs) followed expected routes of circulation and had no undesirable effects. Although administration of 300 mg NPs/kg SNAREs resulted in immediate fatality, the cause of death was due to circulatory failure and mechanical blockage of pulmonary vasculature as determined by gross and histopathological evaluation. Although a dismal outcome, this dosage would need to be evaluated carefully in future studies, especially because the embolization of the vasculature is caused by aggregates of the IONPS. Since no acute iron toxicity was detected at the 150 mg NPs/kg dose, it is possible that much higher doses can be tolerated if administered in multiple consecutive boluses.

In another study, Di Bona et al. (2015) probed the toxicity of IONPs in fetal development based on surface-charge and administered dose. Surface-modified with positively charged PEI or negatively charged poly(acrylic acid) (PAA), the IONPs were injected intraperitonially in pregnant CD-1 mice. On GD 8, 9, or 10 (critical for organogenesis), the NP formulations were administered at a low dose (10 mg NPs/kg) and a high dose (100 mg NPs/kg). The developmental toxicity and biodistribution was investigated for a single dose or multiple doses of either formulation. They observed no significant toxicity at the lower dose for each formulation, but at the higher dose reported significant histological alterations in the uteri and testes. Additionally, significant increases in iron content were reported in the fetal liver and placenta in mice treated with PEI-NPs for eight consecutive doses, but not in the other treatment groups. Further, administration of consecutive doses of either formulation significantly increased frequency of fetal resorption and decreased MGW for PEI-NP treated mice. As such, the authors concluded that the particle charge may play a role in bioaccumulation in the developing fetus. These studies were summarized in Table S8.

The correlation between negatively charged particles and their lack of accumulation in the fetal compartments is consistent with results on our SNAREs, possessing a negative zeta potential, which did not localize significantly in the fetal compartment. The consensus among the different studies is that there is accumulation of iron in the liver, spleen, and lungs. Unsurprisingly, at the highest dosages (30 and 150 mg NPs/kg SNARE), we had a general increase in iron accumulation in all major organs, demonstrating the extensive distribution of the SNAREs. Interestingly, the accumulation of DIONPs and SNAREs at 30 mg NPs/kg were not significantly different for all the organs, suggesting at the size-dependent rather than surface-composition dependent distribution of the nanoparticles.

Upon evading immune activation and potential for phagocytic uptake, nanoparticles are prone to clearance by the liver and the reticuloendothelial system (RES). Ultra-small IONPs (<50 nm in diameter) have been shown to benefit from slower opsonization and clearance while dextran and PEG surface coating of IONPs result in improved stability and blood circulation times (Feng et al., 2018; Singh et al., 2006). Investigating the clearance rate of IONPs, we reported serum total iron concentration similar to saline-treated controls at 24 h postinjection, suggesting clearance of SNAREs. Several other groups have also demonstrated serum iron concentration as an effective measurement of IONPs in the blood and blood clearance at 24 hr (Feng et al., 2018; Sharma et al., 2018). To Elucidate the effect of PEG on NP clearance, we compared the clearance rates by determining the AUC for DIONP- and SNARE-treated dams. We observed larger AUC and thus slower clearance of

SNAREs, suggesting PEG coating plays an important role in circulation times. The optimal circulation time of SNAREs for removal of malicious antibodies from maternal vasculature is unknown. Moreover, it has been reported that PEG size can play a role in prolonging circulation times (Xue et al., 2018). As such, more finetuning of the PEG layer to achieve desirable half-life may be required.

5 | CONCLUSION

This work establishes the basis for the translation of the first ever nanoparticulate prophylactic for MAR autism. Our findings suggested that exposure of pregnant dams to iron oxide nanoparticles does not impose a toxic risk to the mother or the fetus up to the determined MTD. Importantly, no accumulation of nanoparticles was evident in the fetus, which could otherwise jeopardize the development of the fetus. Yet, we are cautious as further studies are needed to investigate any potential side-effects on the developing offspring. In this regard, future studies will focus on assessment of in vivo clearance of MAR autoantibodies in pregnant dams, as well as evaluating colocalization of autoantibodies and nanoparticles via nuclear imaging. Ultimately, we aim to demonstrate therapeutic efficacy in autism mice model (Judy Van de Water et al., 2018) by investigating behavioral changes in offspring of treated dams. As cases of autism are on the rise, we believe we have taken the first step in developing the first prophylactic for ASD, affecting 1 in 59 children born in the United States.

Supplementary Material

Refer to Web version on PubMed Central for supplementary material.

ACKNOWLEDGMENTS

The authors gratefully thank Mr. Charles M. Smith, and Dr. Rachel D. Brownlee for providing time, reagents, and help in performing and training for I.V. injections. Additionally, we thank Dr. Abhijit Chaudhari and Dr. Douglas Rowland for providing time, training and assisting with MRI. Further, we appreciate Mr. Eugene Dunn and Brett Moore at the UCD Comparative Pathology Lab for performing blood chemistry analysis and mice immunization. We would like to also thank Prof. Alyssa Panitch for sharing her Keyence BZX-100 microscope for automated high-resolution imaging of Prussian Blue stained microscope slides.

Dr. Natalia Vapniarsky was supported by the National Center for Advancing Translational Sciences, National Institutes of Health, Institutional Career Development Grant number KL2 TR001859. Professor Jamal Lewis was supported by the grants from the National Institute of General Medical Sciences (1R35GM125012) and National Institute of Allergy and Infectious Disease (1R01AI139399).

REFERENCES

Ali Noori KP, Modaresi M, Messripour M, Yousefi MH, & Amiri GR (2011). Effect of magnetic iron oxide nanoparticles on pregnancy and testicular development of mice. African Journal of Biotechnology, 10(7), 1221–1227.

Athie-Morales V, Smits HH, Cantrell DA, & Hilkens CM (2004). Sustained IL-12 signaling is required for Th1 development. Journal of Immunology, 172(1), 61–69.

Banobre-Lopez M, Teijeiro A, & Rivas J (2013). Magnetic nanoparticle-based hyperthermia for cancer treatment. Reports of Practical Oncology and Radiotherapy, 18(6), 397–400. [PubMed: 24416585]

Biederer J, Beer M, Hirsch W, Wild J, Fabel M, Puderbach M, & van Beek EJR (2012). MRI of the lung (2/3). Why … when … how? Insights Imaging, 3(4), 355–371. [PubMed: 22695944]

Bolandparvaz A, Harriman R, Alvarez K, Lilova K, Zang Z, Lam A, … Lewis J (2019). Towards a nanoparticle-based prophylactic for maternal autoantibody-related autism. Nanomedicine, 21, 102067. [PubMed: 31349087]

Braunschweig D, Krakowiak P, Duncanson P, Boyce R, Hansen RL, Ashwood P, … van de Water J (2013). Autism-specific maternal autoantibodies recognize critical proteins in developing brain. Translational Psychiatry, 3, e277. [PubMed: 23838888]

Bungener L, Serre K, Bijl L, Leserman L, Wilschut J, Daemen T, & Machy P (2002). Virosome-mediated delivery of protein antigens to dendritic cells. Vaccine, 20(17–18), 2287–2295. [PubMed: 12009284]

Carson FL (2009). Histotechnology: A self-instructional text (3rd ed.). Chicago, Illinois: American Society for Clinical Patho.

Chaste P, & Leboyer M (2012). Autism risk factors: Genes, environment, and gene-environment interactions. Dialogues in Clinical Neuroscience, 14(3), 281–292. [PubMed: 23226953]

Chernoff N, Rogers EH, Gage MI, & Francis BM (2008). The relationship of maternal and fetal toxicity in developmental toxicology bioassays with notes on the biological significance of the “no observed adverse effect level”. Reproductive Toxicology, 25(2), 192–202. [PubMed: 18242052]

Chiou WL, & Hsu FH (1975). Pharmacokinetics of creatinine in man and its implications in the monitoring of renal function and in dosage regimen modifications in patients with renal insufficiency. Journal of Clinical Pharmacology, 15(5–6), 427–434. [PubMed: 1133219]

Cook N, Hansen AR, Siu LL, & Abdul Razak AR (2015). Early phase clinical trials to identify optimal dosing and safety. Molecular Oncology, 9(5), 997–1007. [PubMed: 25160636]

Di Bona KR, Xu Y, Gray M, Fair D, Hayles H, Milad L, … Rasco JF (2015). Short- and long-term effects of prenatal exposure to iron oxide nanoparticles: Influence of surface charge and dose on developmental and reproductive toxicity. International Journal of Molecular Sciences, 16(12), 30251–30268. [PubMed: 26694381]

Feng Q, Liu Y, Huang J, Chen K, Huang J, & Xiao K (2018). Uptake, distribution, clearance, and toxicity of iron oxide nanoparticles with different sizes and coatings. Scientific Reports, 8(1), 2082. [PubMed: 29391477]

Fox-Edmiston E, & Van de Water J (2015). Maternal anti-fetal brain IgG autoantibodies and autism Spectrum disorder: Current knowledge and its implications for potential therapeutics. CNS Drugs, 29(9), 715–724. [PubMed: 26369920]

Garty BZ, Ludomirsky A, Danon YL, Peter JB, & Douglas SD (1994). Placental transfer of immunoglobulin G subclasses. Clinical and Diagnostic Laboratory Immunology, 1(6), 667–669. [PubMed: 8556518]

Ghasempour S, Shokrgozar MA, Ghasempour R, & Alipour M (2015). Investigating the cytotoxicity of iron oxide nanoparticles in in vivo and in vitro studies. Experimental and Toxicologic Pathology, 67(10), 509–515. [PubMed: 26279467]

Gowda S, Desai PB, Hull VV, Math AA, Vernekar SN, & Kulkarni SS (2009). A review on laboratory liver function tests. The Pan African Medical Journal, 3, 17. [PubMed: 21532726]

Gu L, Fang RH, Sailor MJ, & Park JH (2012). In vivo clearance and toxicity of monodisperse iron oxide nanocrystals. ACS Nano, 6(6), 4947–4954. [PubMed: 22646927]

Hu CM, Zhang L, Aryal S, Cheung C, Fang RH, & Zhang L (2011). Erythrocyte membrane-camouflaged polymeric nanoparticles as a biomimetic delivery platform. Proceedings of the National Academy of Sciences of the United States of America, 108(27), 10980–10985. [PubMed: 21690347]

Jarrett BR, Frendo M, Vogan J, & Louie AY (2007). Size-controlled synthesis of dextran sulfate coated iron oxide nanoparticles for magnetic resonance imaging. Nanotechnology, 18(3), 035603. [PubMed: 19636126]

Baio J, Wiggins L, Christensen DL, Maenner MJ, Daniels J, Warren Z, … Dowling NF (2018). Prevalence of autism spectrum disorder among children aged 8 years—autism and developmental disabilities monitoring network, 11 sites, United States, 2014. Centers for Disease Control and Prevention, 67(6), 1–23.

Van de Water Judy, J. KL, Silverman J, Yang M, & Crawley J (2018). Autism-specific maternal autoantibodies produce ASD relevant behaviors in a mouse model. Biological Psychiatry, 83(9), S147–S148.

Kami D, Takeda S, Itakura Y, Gojo S, Watanabe M, & Toyoda M (2011). Application of magnetic nanoparticles to gene delivery. International Journal of Molecular Sciences, 12(6), 3705–3722. [PubMed: 21747701]

Kermanizadeh A, Vranic S, Boland S, Moreau K, Baeza-Squiban A, Gaiser BK, … Stone V (2013). An in vitro assessment of panel of engineered nanomaterials using a human renal cell line: Cytotoxicity, pro-inflammatory response, oxidative stress and genotoxicity. BMC Nephrology, 14, 96. [PubMed: 23617532]

Lewis JS, Dolgova NV, Chancellor TJ, Acharya AP, Karpiak JV, Lele TP, & Keselowsky BG (2013). The effect of cyclic mechanical strain on activation of dendritic cells cultured on adhesive substrates. Biomaterials, 34(36), 9063–9070. [PubMed: 24008042]

Lu AH, Salabas EL, & Schuth F (2007). Magnetic nanoparticles: Synthesis, protection, functionalization, and application. Angewandte Chemie (International Ed. in English), 46(8), 1222–1244. [PubMed: 17278160]

Lu M, Cohen MH, Rieves D, & Pazdur R (2010). FDA report: Ferumoxytol for intravenous iron therapy in adult patients with chronic kidney disease. American Journal of Hematology, 85(5), 315–319. [PubMed: 20201089]

Ma X, Yan W, Zheng H, Du Q, Zhang L, Ban Y, … Wei F (2015). Regulation of IL-10 and IL-12 production and function in macrophages and dendritic cells. F1000Research, 4(F1000 Faculty Rev), 1465.

Meltzer A, & Van de Water J (2017). The role of the immune system in autism Spectrum disorder. Neuropsychopharmacology, 42(1), 284–298. [PubMed: 27534269]

NC3Rs. n.d. How much blood does a mouse have? https://www.nc3rs.org.uk/mouse-decision-tree-blood-sampling.

Neto LMMZN, de Sousa-Júnior T, da Costa B, & Kipnis J-K (2018). Specific T cell induction using iron oxide based nanoparticles as subunit vaccine adjuvant. Human Vaccines & Immunotherapeutics, 14(11), 2786–2801. [PubMed: 29913109]

Park EJ, Oh SY, Kim Y, Yoon C, Lee BS, Kim SD, & Kim JS (2016). Distribution and immunotoxicity by intravenous injection of iron nanoparticles in a murine model. Journal of Applied Toxicology, 36 (3), 414–423. [PubMed: 26416317]

Pompei L, Jang S, Zamlynny B, Ravikumar S, McBride A, Hickman SP, & Salgame P (2007). Disparity in IL-12 release in dendritic cells and macrophages in response to *Mycobacterium tuberculosis* is due to use of distinct TLRs. Journal of Immunology, 178(8), 5192–5199.

Riley P, Allen AB, Jeffrey AM, Manickam VA, & Lewis Latent JS (2018). Immunosuppressive nature of poly(lactic-co-glycolic acid) microparticles. ACS Biomaterial Science and Engineering, 4(3), 900–918.

Rojas JM, Sanz-Ortega L, Mulens-Arias V, Gutierrez L, Perez-Yague S, & Barber DF (2016). Superparamagnetic iron oxide nanoparticle uptake alters M2 macrophage phenotype, iron metabolism, migration and invasion. Nanomedicine, 12(4), 1127–1138. [PubMed: 26733263]

Santos EWO, de Cunha D, Hastreiter A, da Silva GB, Beltran J. S. d. O., Tsujita M, … Neves S (2016). Hematological and biochemical reference values for C57BL/6, Swiss Webster and BALB/c mice. Brazilian Journal of Veterinary Research and Animal Science, 53(2), 138–145.

Sharma A, Cornejo C, Mihalic J, Geyh A, Bordelon DE, Korangath P, … Ivkov R (2018). Physical characterization and in vivo organ distribution of coated iron oxide nanoparticles. Scientific Reports, 8(1), 4916. [PubMed: 29559734]

Singh R, Pantarotto D, Lacerda L, Pastorin G, Klumpp C, Prato M, … Kostarelos K (2006). Tissue biodistribution and blood clearance rates of intravenously administered carbon nanotube radiotracers. Proceedings of the National Academy of Sciences of the United States of America, 103(9), 3357–3362. [PubMed: 16492781]

Stephen ZR, Kievit FM, & Zhang M (2011). Magnetite nanoparticles for medical MR imaging. Mater Today (Kidlington), 14 (7–8), 330–338. [PubMed: 22389583]

Townsley MI (2012). Structure and composition of pulmonary arteries, capillaries, and veins. Comprehensive Physiology, 2(1), 675–709. [PubMed: 23606929]

Unterweger H, Janko C, Schwarz M, Dézsi L, Urbanics R, Matuszak J, … Cicha I (2017). Non-immunogenic dextran-coated superparamagnetic iron oxide nanoparticles: A biocompatible, size-tunable contrast agent for magnetic resonance imaging. International Journal of Nanomedicine, 12, 5223–5238. [PubMed: 28769560]

Vinay Kumar NS, & Maitra SS (2017). In vitro and in vivo toxicity assessment of nanoparticles. International Nano Letters, 7(4), 243–256.

Wang YX (2015). Current status of superparamagnetic iron oxide contrast agents for liver magnetic resonance imaging. World Journal of Gastroenterology, 21(47), 13400–13402. [PubMed: 26715826]

Williams White S, Keonig K, & Scahill L (2007). Social skills development in children with autism spectrum disorders: A review of the intervention research. Journal of Autism and Developmental Disorders, 37(10), 1858–1868. [PubMed: 17195104]

Wu W, Wu Z, Yu T, Jiang C, & Kim WS (2015). Recent progress on magnetic iron oxide nanoparticles: Synthesis, surface functional strategies and biomedical applications. Science and Technology of Advanced Materials, 16(2), 023501. [PubMed: 27877761]

Xue W, Liu Y, Zhang N, Yao Y, Ma P, Wen H, … Fan H (2018). Effects of core size and PEG coating layer of iron oxide nanoparticles on the distribution and metabolism in mice. International Journal of Nanomedicine, 13, 5719–5731. [PubMed: 30310275]

Zhang Q, Zeng SX, & Lu H (2015). Determination of maximum tolerated dose and toxicity of Inauhzin in mice. Toxicology Reports, 2, 546–554. [PubMed: 26167454]

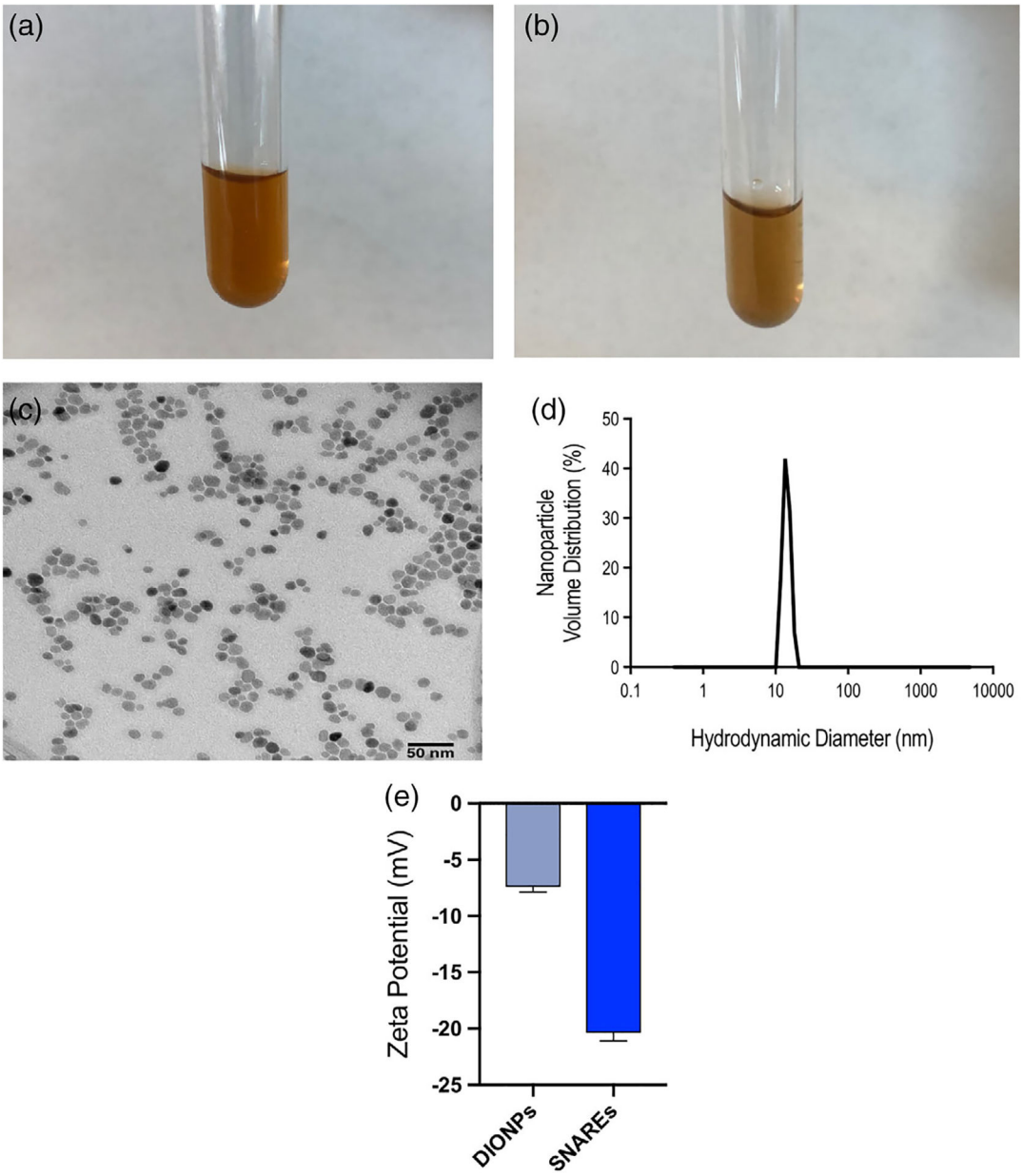

FIGURE 1.

Physico-chemical characterization of iron oxide nanoparticles and SNAREs. Images of (a) DIONPs and (b) SNAREs at 1 mg/mL dispersed in water. (c) Transmission Electron Microscopy (TEM) of DIONPs. (d) Dynamic Light Scattering (DLS) of DIONPs. (e) The zeta potential of 1 mg/ml of DIONPs and SNAREs in water at physiological temperature

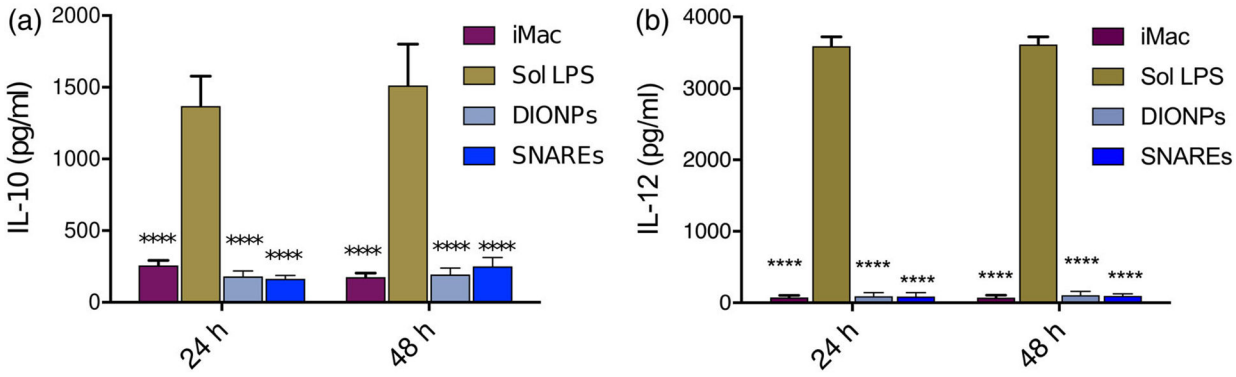

FIGURE 2.

Investigating IL-10 and IL-12 release from bone marrow-derived macrophages in the presence of DIONPs and SNAREs. **(a)** ELISA on treatment supernatants and immature macrophages demonstrated significantly lower secretion of IL-10 compared to LPS-treated macrophages at 24 and 48 hr. **(b)** Supernatant from immature macrophages as well as DIONP and SNARE treated cultures showed lowered secretion of IL-12 compared to LPS-treated cells at same time points. The mean of every treatment was compared to LPS treatments and significance is denoted by (****) for $p < .0001$

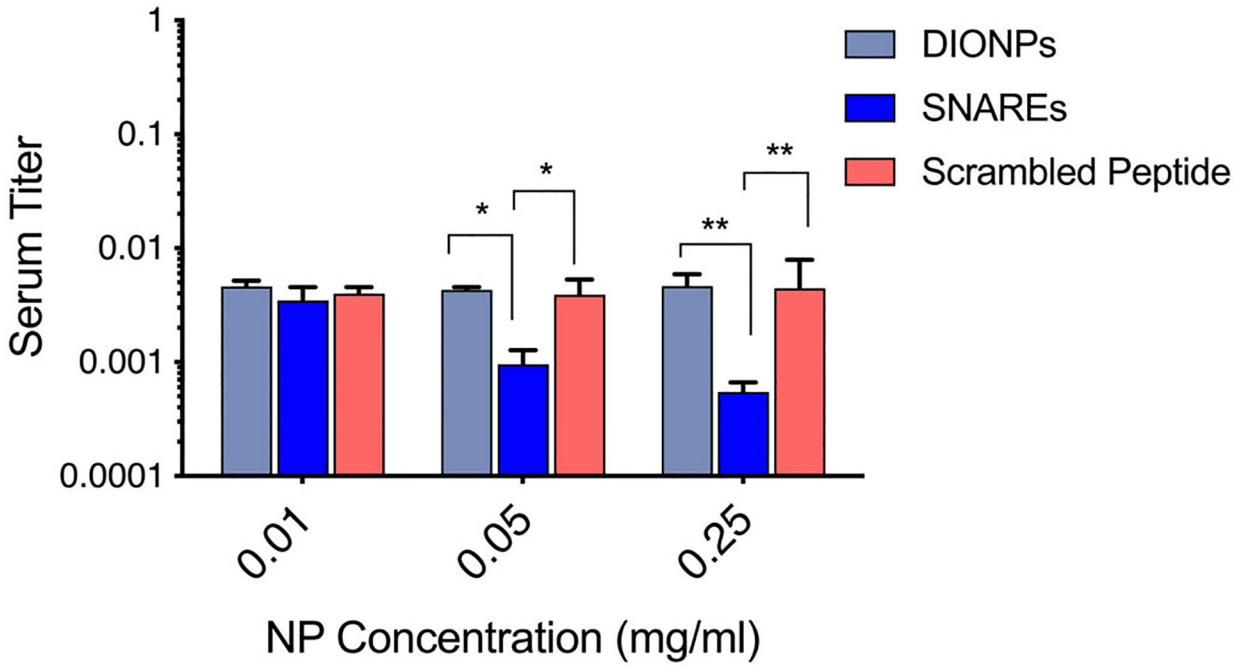

FIGURE 3.

Capture of MAR LDH B autoantibody from mouse serum. SNAREs significantly reduced LDH B antibody titer in mouse serum by capturing up to 87% of LDH B antibodies in vitro. Scrambled peptide-modified DIONPs and plain DIONPs served as negative controls. Data shown represent mean ± standard error ($n = 3$ biological replicates). The mean of every treatment was compared to the control and significance is denoted by (*) for $p < .05$ and (***) for $p < .001$

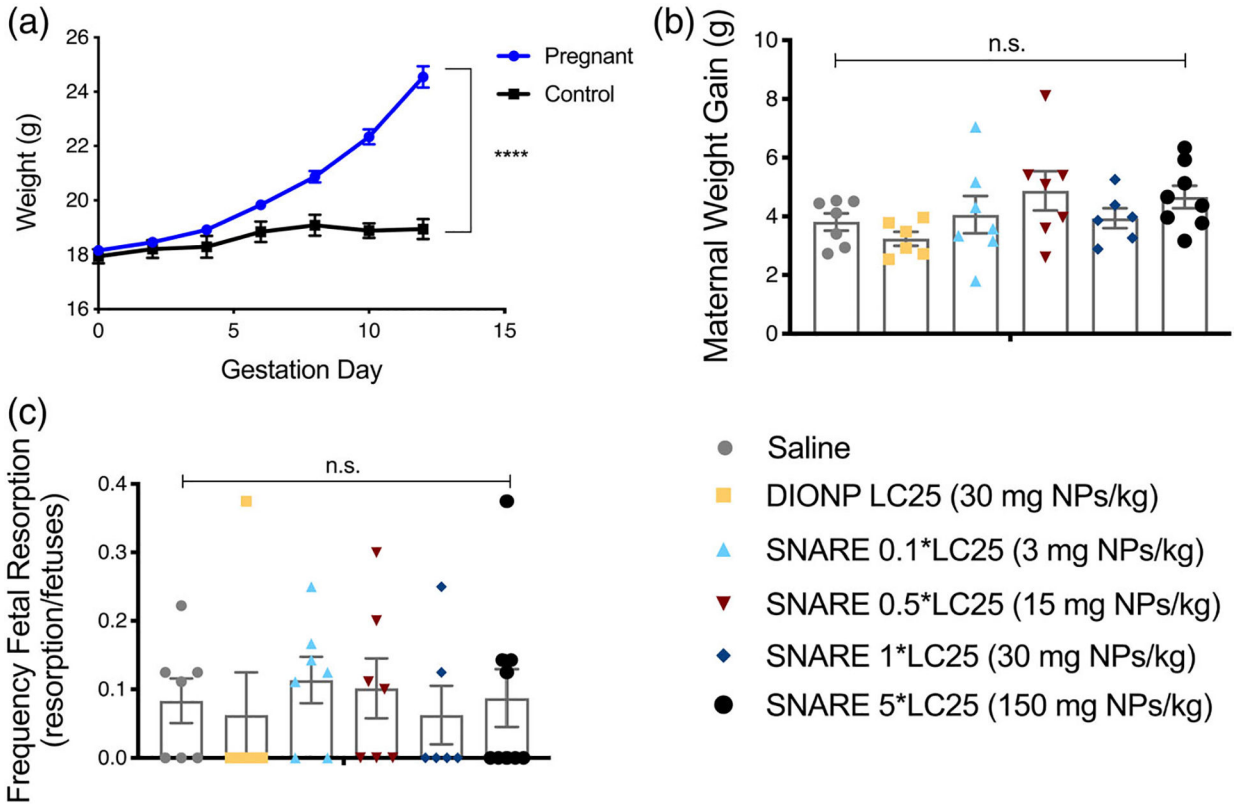

FIGURE 4.

Maternal and Fetal toxicity of SNAREs and DIONPs in pregnant dams. (a) Weight gain of a subset of pergnant dams ($n = 55$) from GD 0 to GD 12 compared to unmated control ($n = 7$). Weight gain was used as a second confimatory parameter asides from observing copulation plug to establish timed pregnancies. The weight of pregnant dams were signficiantly different at GD 17 compared to the control. (b) Maternal weight gain determined by subtracting the weight of the dam at GD 0 and uteri on GD 17 from the weight of the dam at GD 17. (c) Frequency of fetal resorption calculated as number of resorption/number of fetuses of treated compared to control mice. Legend applies to graphs b,c

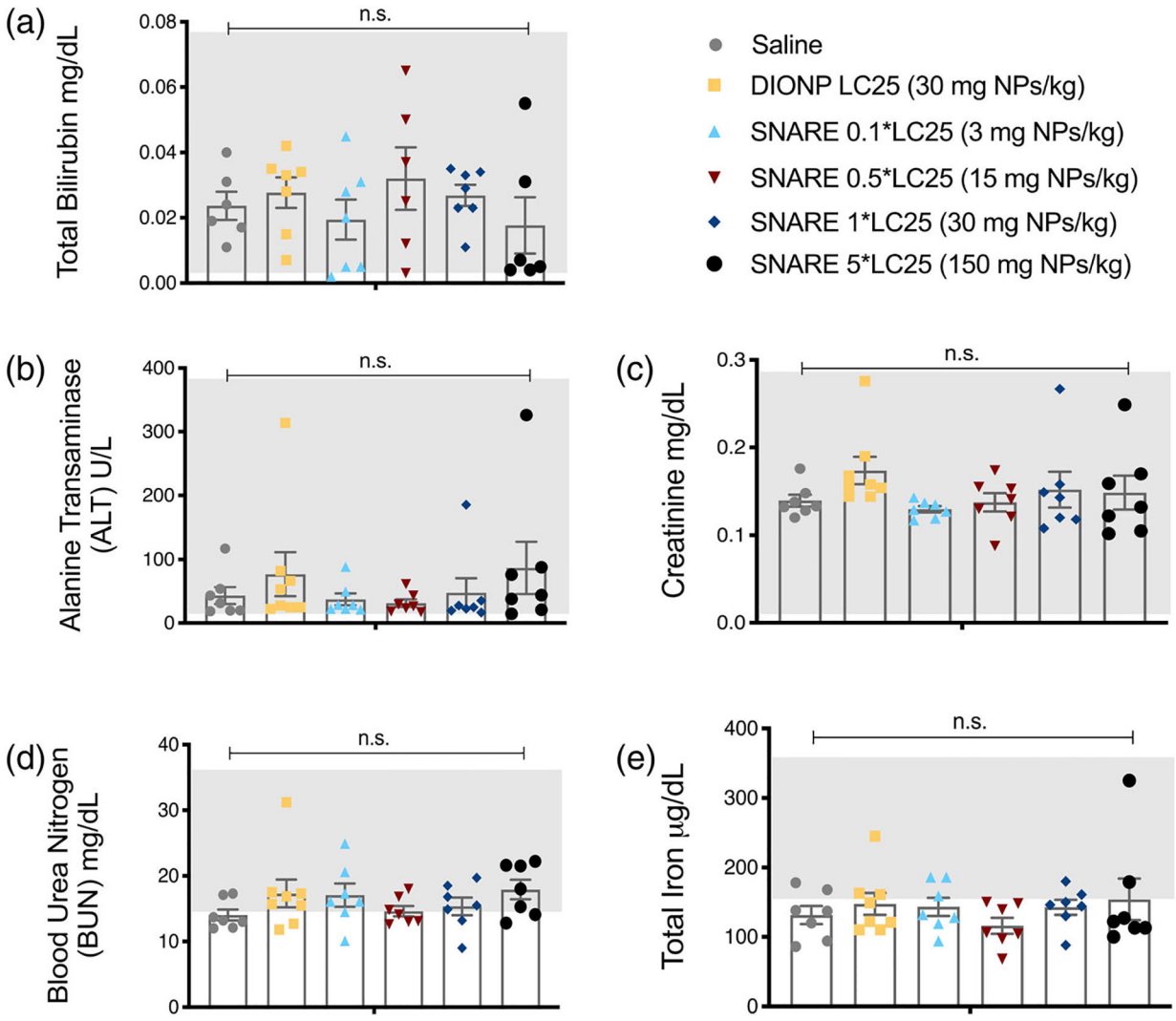

FIGURE 5.

Serum biochemical composition of pregnant mice treated with SNAREs and DIONPs. Serum composition of total Bilirubin, Alanine Transaminase (ALT), Creatinine, Blood Urea Nitrogen (BUN), and total Iron of treated and control mice assessing liver and kidney functionalities. Blood was collected via cardiac puncture on GD 17 and serum separated via centrifugation in gel separator yellow-capped tubes. (a) Total bilirubin (range: 0–0.2 mg/dl). (b) Alanine transaminase (ALT) (range: 0–403 U/L). (c) Creatinine (range: 0–0.3 mg/dl). (d) Blood urea nitrogen (range: 15.2–34.7 mg/dl). (e) Total iron (range: 176–347 µg/dl). Legend applies to all graphs. Ranges shown grey dervied from nonpregnant BALB/c strain mice from UCD Pathology lab

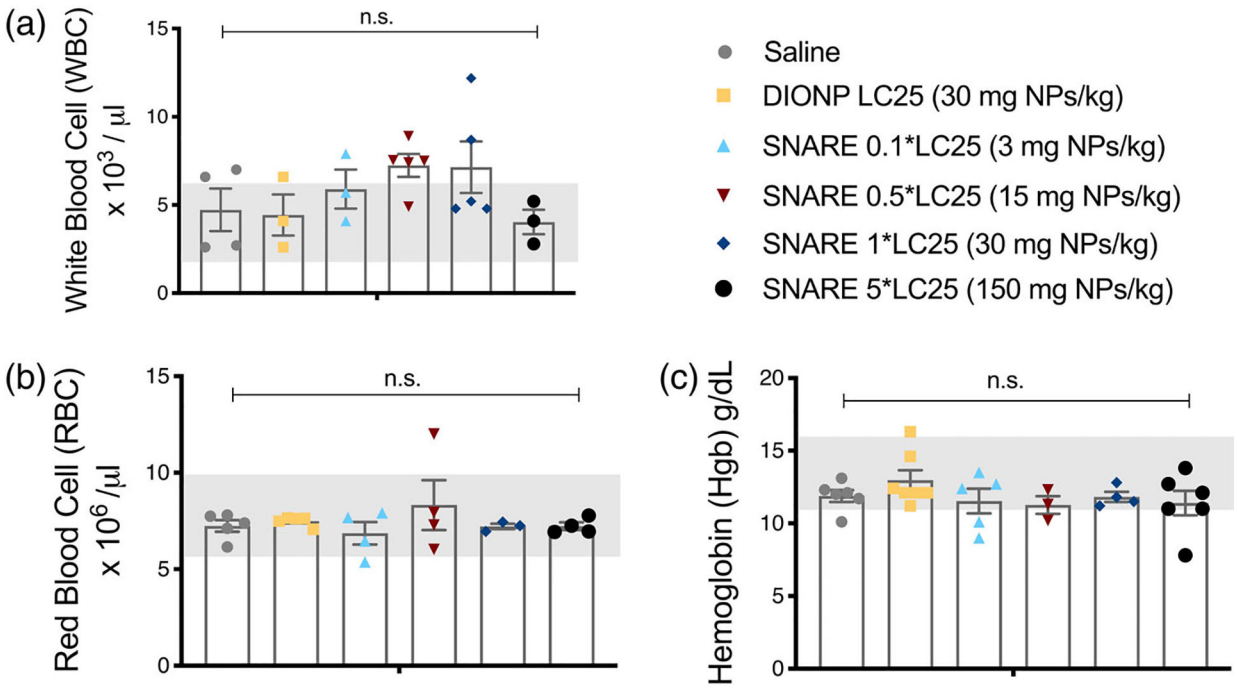

FIGURE 6.

Hematological analysis of SNARE and DIONP-treated mice. Blood count of white blood cells (WBC), red blood cells (RBC), and hemoglobin (Hgb) of treated and control mice. Blood was collected via cardiac Puncture on GD 17 and serum separated via centrifugation in gel separator yellow-capped tubes. (a) WBC, (b) RBC, (c) Hgb. Legend applies to all graphs. Reference range for nonpregnant C57BL/6j shown in grey (Santos et al., 2016)

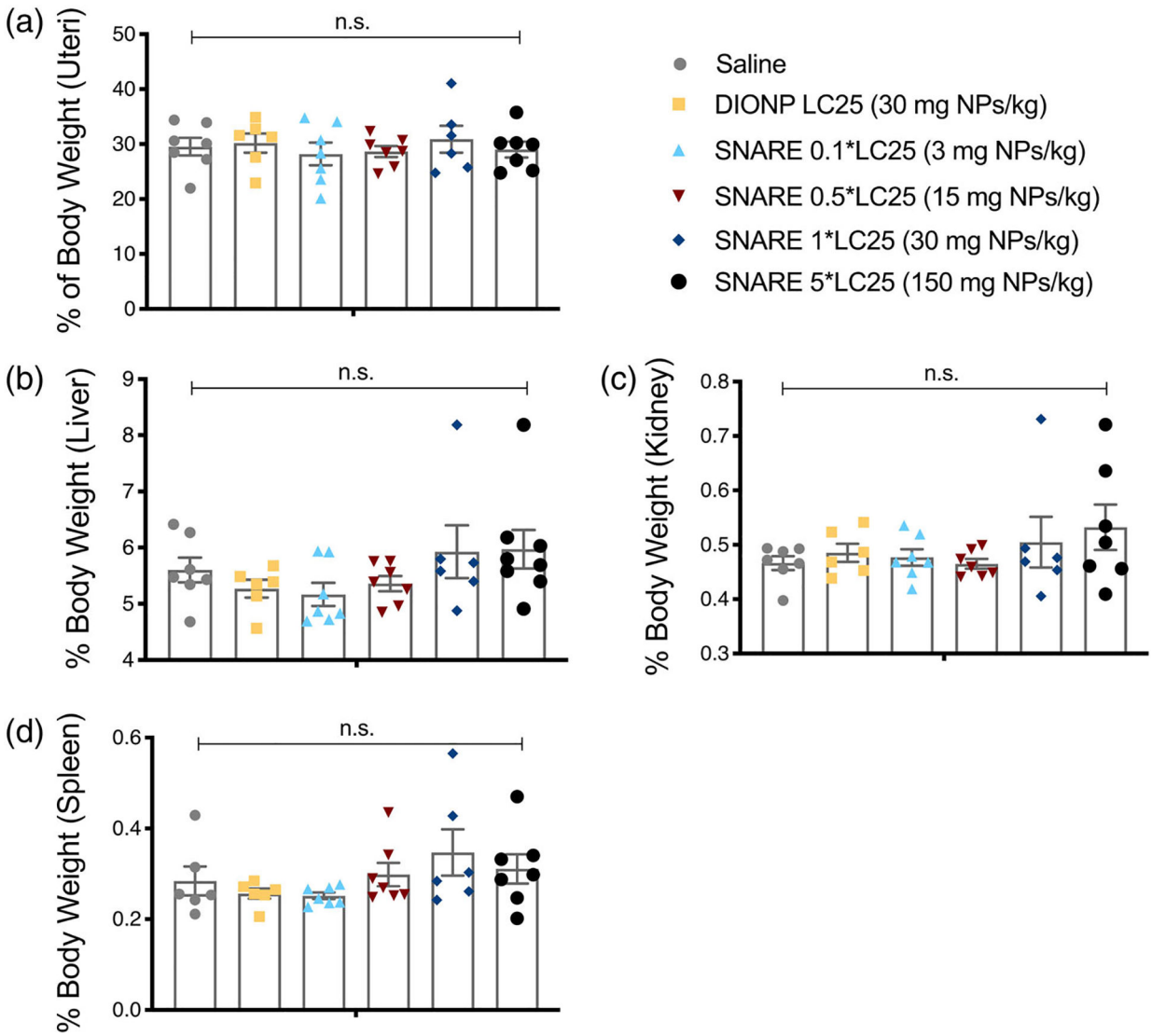

FIGURE 7.

Percent body weight of major maternal organs upon necropsy on gestational day 17. Percent body weight on GD 17 of uteri, liver, kidneys, spleen of treated and control mice assessing toxicity-related weight changes in major organs involved in clearance of iron oxide nanoparticles. (a) Uteri, (b) Liver, (c) Kidneys, (d) Spleen. Legend applies to all graphs

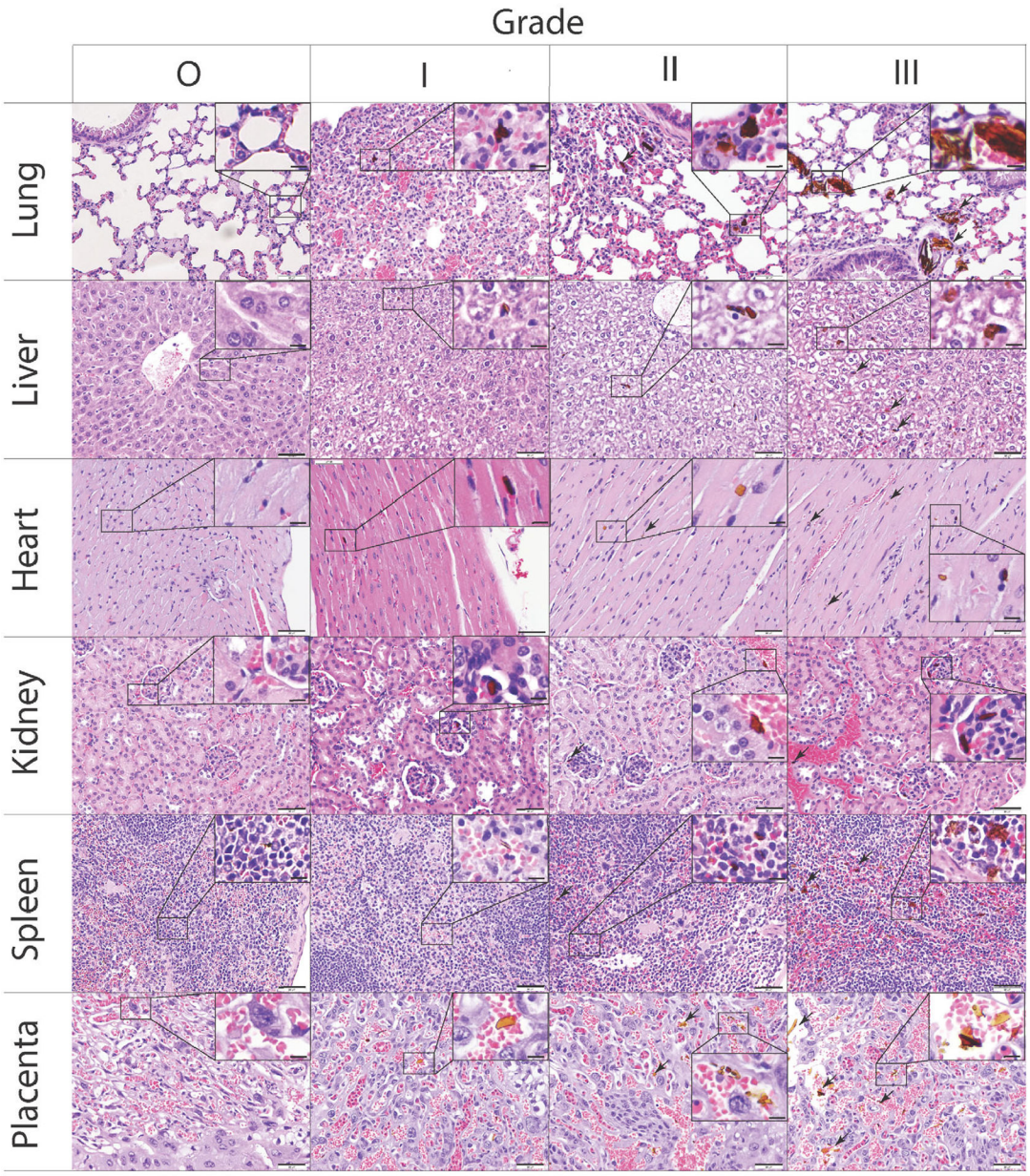

FIGURE 8.

Representative histological images of major organs and their grades. In Grade 0, no iron aggregates are present in any of the organs shown. Hepatocytes are occasionally binucleated (inset), which is a typical feature of the murine liver. In the spleen, physiological iron accumulation is shown in the macrophage of the red pulp (inset). In Grade I, one iron aggregate was detected per ×20 power field. In the lung, these aggregates were present within pulmonary capillaries (inset). In the liver, iron deposits were primarily observed within Kupffer cells (inset). In the heart, rare iron aggregates were present within coronary capillaries. In the kidney, iron aggregates were rarely seen within glomerular tuft capillaries (inset). In the placenta, iron aggregates were observed within intervillous blood channels. In Grade II, there were 2–3 iron aggregates per ×20 power field. In the lung, these aggregates

were present only within pulmonary capillaries (inset). In the liver, aggregates were associated with Kupffer cells but occasionally were also observed within the sinusoids. In the heart, the aggregates were restricted to the coronary capillaries (inset and arrow). In the kidney, aggregates were primarily observed within glomerular tuft capillaries (arrow) and rarely within renal vasculature (inset). In Grade III, >3 iron aggregates were observed per ×20 power field, with no evidence of inflammation, cellular damage, or histomorphological change to the organ architecture. In the lung, multiple pulmonary capillaries are distended and occluded by large iron aggregates (arrows and inset). In the liver, Kupffer cells are enlarged with phagocytosed iron (inset), and occasional sinusoids contain cigar-shaped aggregates (arrows). In the heart, the iron aggregates are present within coronary capillaries (inset) but occasionally within the ventricles (not shown). In the kidney, the aggregates are observed within glomerular tufts (inset) capillaries and sometimes within vasa recta (arrow). The spleen contains abundant and above physiological iron deposits within rep pulp macrophages (inset and arrows). In the placental sections, variably sized iron aggregates are present within intervillous spaces (inset and arrows). The criteria of Grade IV and V included evidence of inflammation and inflammation associated with gross or histological alteration of organ morphology, respectively. In this study, no Grades IV or V were assigned to any of the examined tissues. Staining: Hematoxylin and eosin, Bar = 50 μm, and 10 μm in the insets

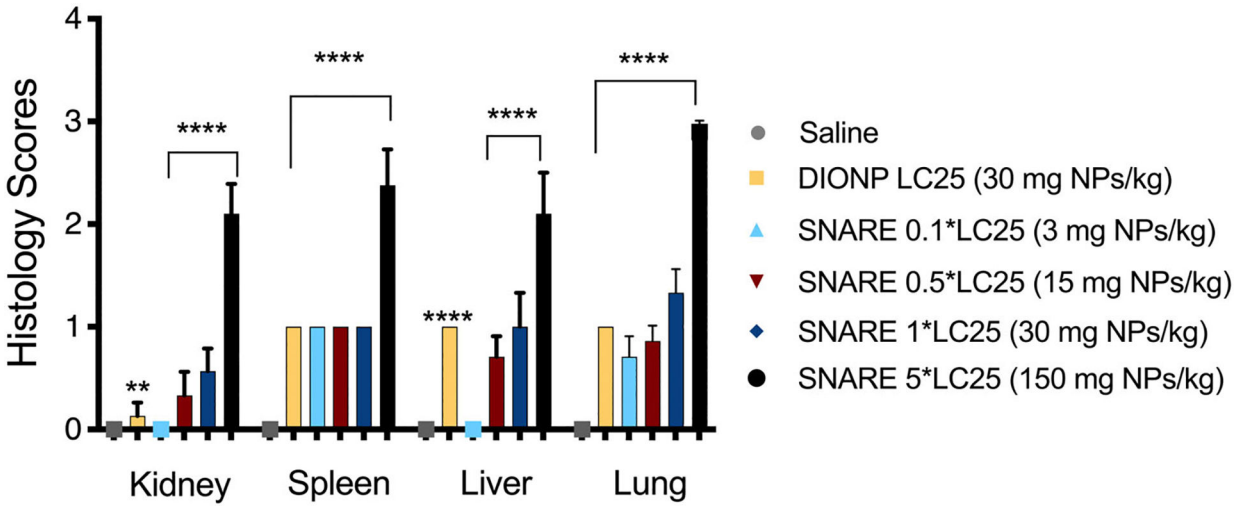

FIGURE 9.

Histological grading for the major maternal organs at the different dosages. The grades were assigned based on acute inflammation and potential tissue damage. There is significant accumulation at the MTD dose and thus highest grading. Data shown represent mean ± standard error ($n \leq 3$ biological replicates). The mean of every treatment was compared to the control group and significance is denoted by (**) for $p < .01$ and (****) for $p < .0001$

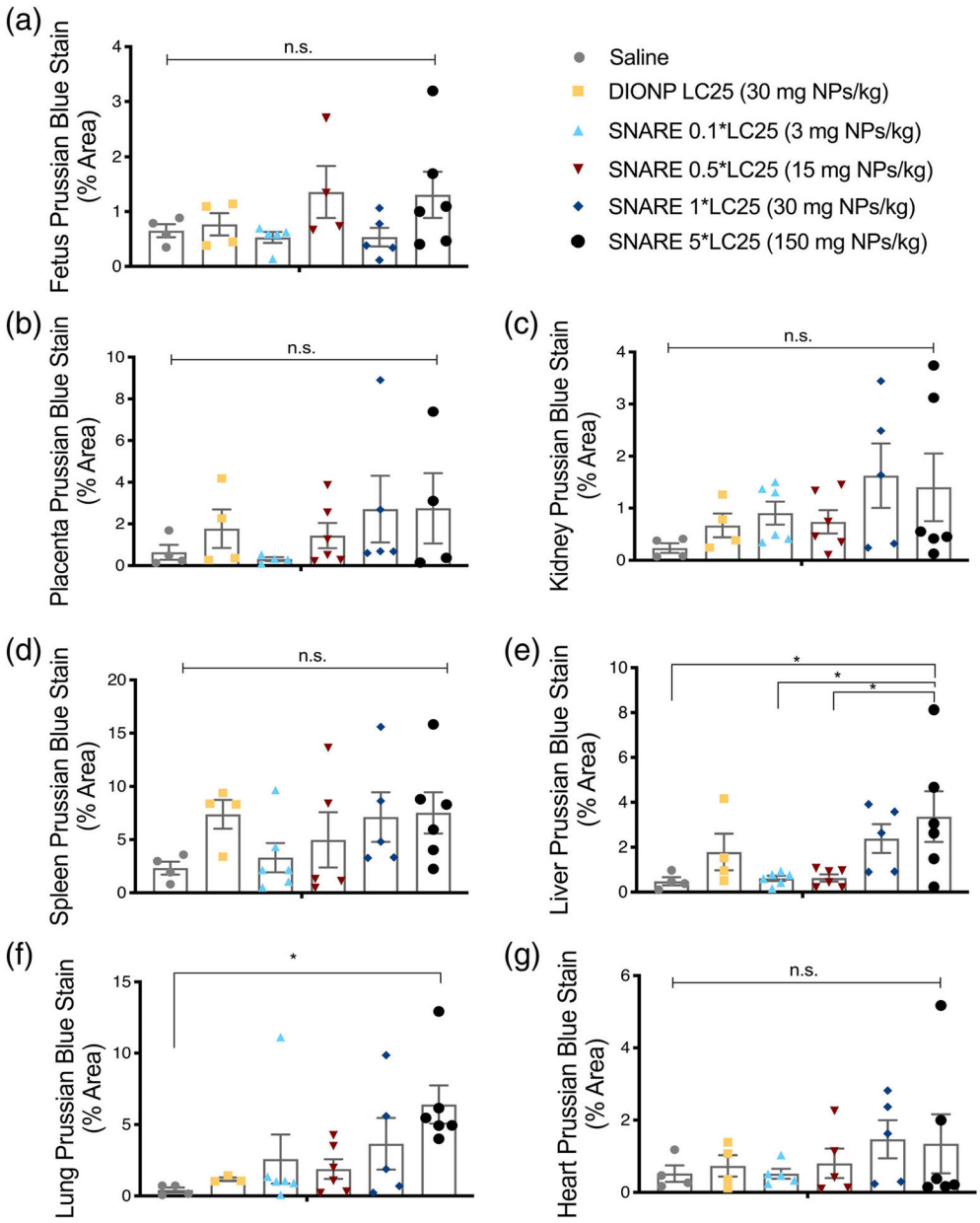

FIGURE 10.

Prussian Blue iron stain of maternal organs to determine organ iron accumulation. Prussian Blue iron stain and a nuclear fast red counter-stain of maternal organs comparing treatments versus saline control. Tissues were embedded, sectioned, and stained for iron after necropsy on gestational day 17. There was a general accumulation of iron in the maternal organs at the 30 and 150 mg NPs/kg of SNAREs as well as 30 mg NPs/kg DIONPs. There was a significant increase of iron in the maternal liver and the lungs at the MTD dose of 150 mg NPs/kg compared to the saline-treated dams. (a) Fetus, (b) placenta, (c) kidneys, (d) spleen, (e) liver, (f) lungs, (g) heart

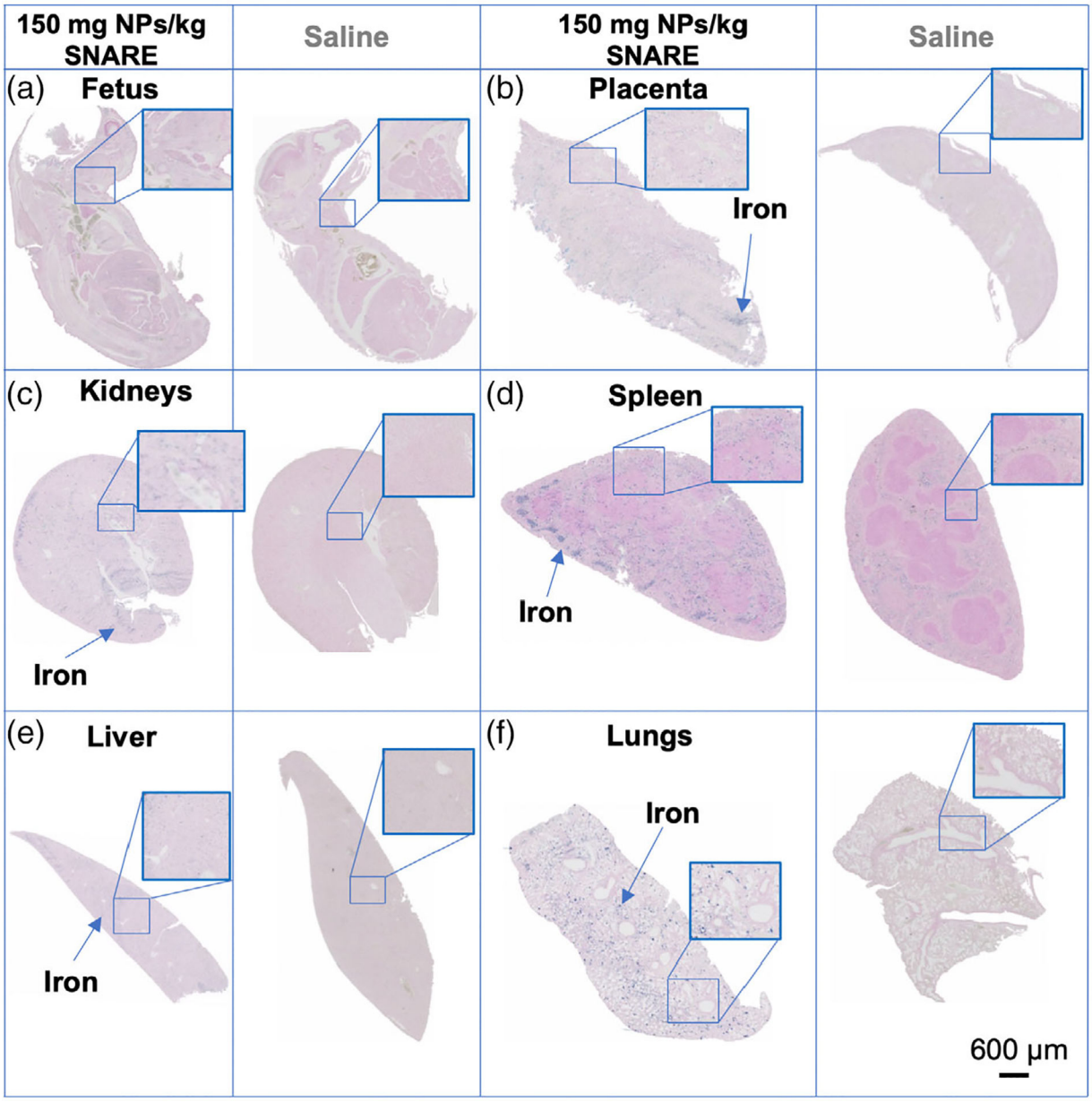

FIGURE 11.

Representative images of Prussian Blue iron stain of maternal organs and fetus. Representative images (×4 magnification) of Prussian Blue iron stain and a nuclear fast counter stain of maternal organs and fetus comparing 150 mg NPs/kg SNARE treatment versus saline control. Arrows point to the accumulation of iron in the organs. Tissues were embedded, sectioned, and stained for iron after necropsy on GD 17. There was a general accumulation of iron at the 150 mg NPs/kg of SNAREs compared to the saline control for the different organs with a significant increase for the liver and the lungs compared to the saline control. (a) Fetus, (b) placenta, (c) kidneys, (d) spleen (E) liver (F) lungs

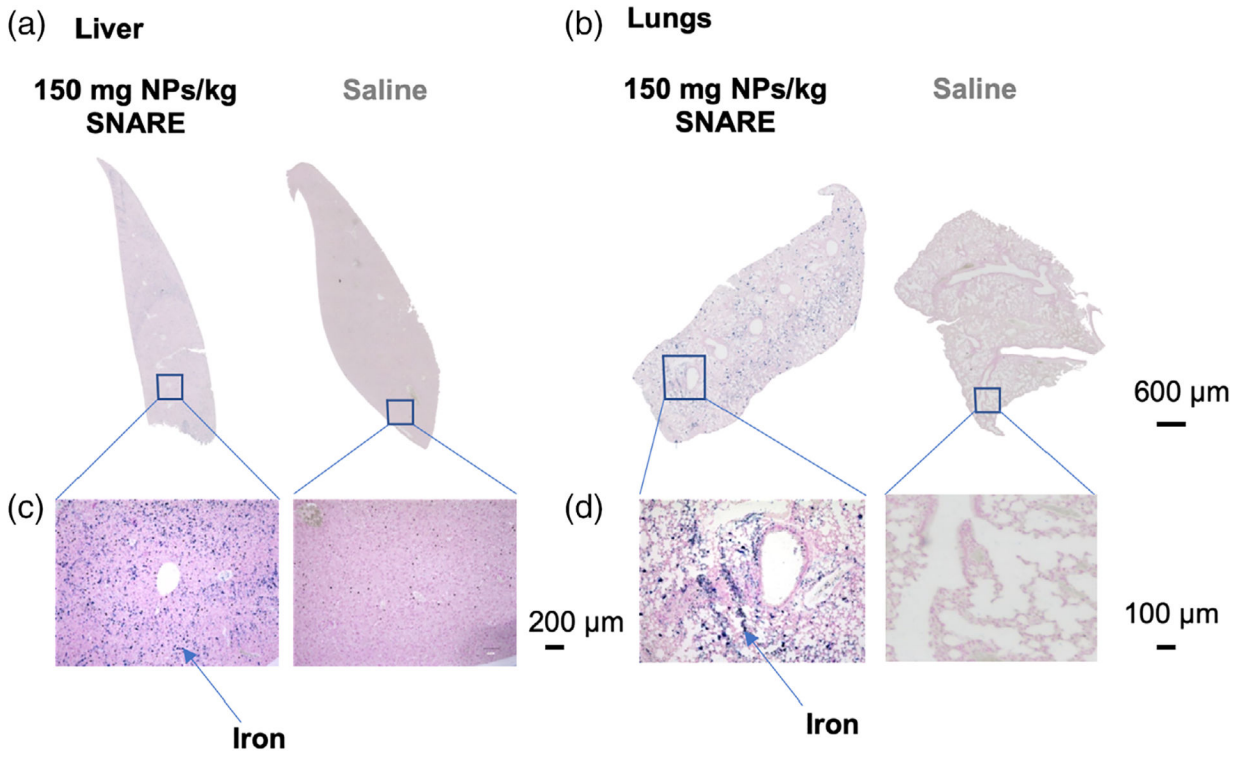

FIGURE 12.

Representative images of Prussian Blue iron stain of maternal lungs and liver. Representative images (×4, ×10) of Prussian Blue iron stain and a nuclear fast counter stain of maternal organs comparing 150 mg NPs/kg SNARE treatment versus saline-treated control. Arrows point to the accumulation of iron in the organs. Tissues were embedded, sectioned, and stained for iron after necropsy on GD 17. There was a general accumulation of iron at the 150 mg NPs/kg of SNAREs compared to the saline-treated control for the different organs with a significant increase in the liver and the lungs. (a) ×4 Magnification liver, (b) ×4 magnification lungs, (c) ×10 magnification liver, (d) ×20 magnification lungs

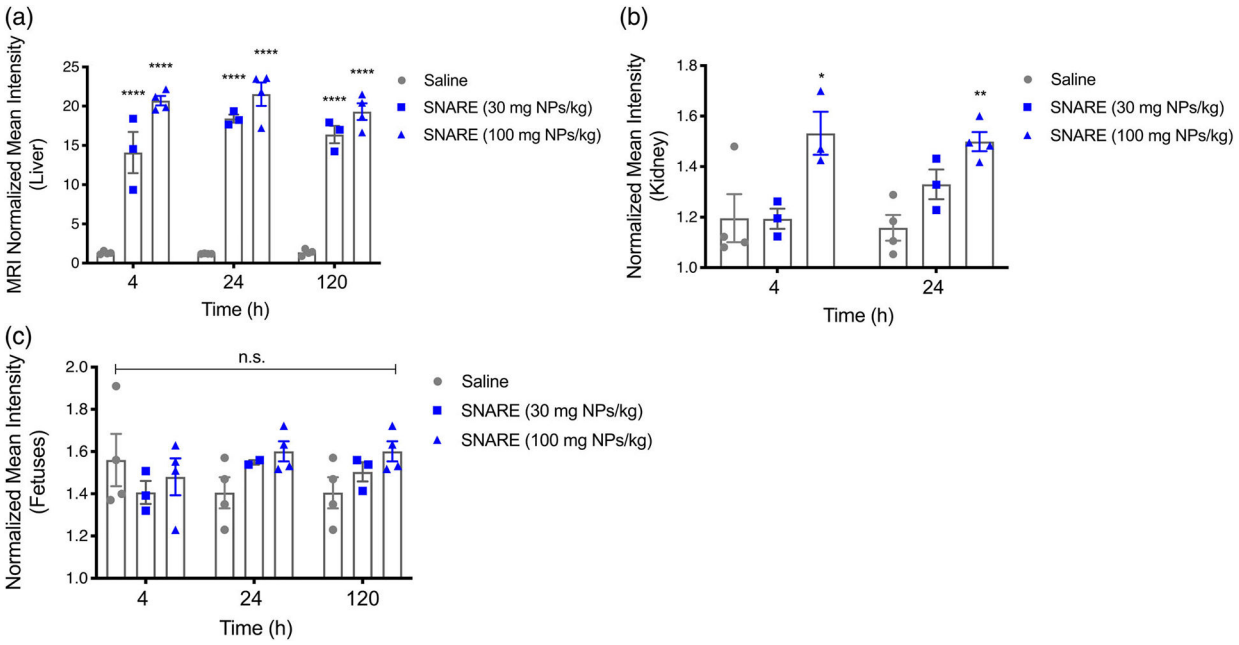

FIGURE 13.

Distribution of intravenously injected SNAREs in pregnant dams via MRI. Pregnant dams were administered with 30 and 100 mg NPs/kg SNAREs, slightly lower doses than the MTD (150 mg NPs/kg). Distribution of NPs in the maternal liver (a) and kidney (b) as well as fetuses (c) was investigated at 24, 48 hr and 5 days postinjection via MRI. The liver demonstrated significant accumulation of NPs at both doses by 4 hr and persisted up to 5 days. Kidneys exhibited significant deposition at only the higher dose by 4 hr and remained present up to 24 hr, but the large size of the fetuses by Day 5 blocked MRI acquisition of the kidneys. Data were analyzed using Slicer software and mean intensity normalized to a water capillary tube to ensure comparability across images. Data shown represent mean ± standard error ($n \geq 3$ biological replicates). The mean of every treatment was compared to each other and the controls and significance is denoted by (*) for $p < .05$ and (****) for $p < .0001$

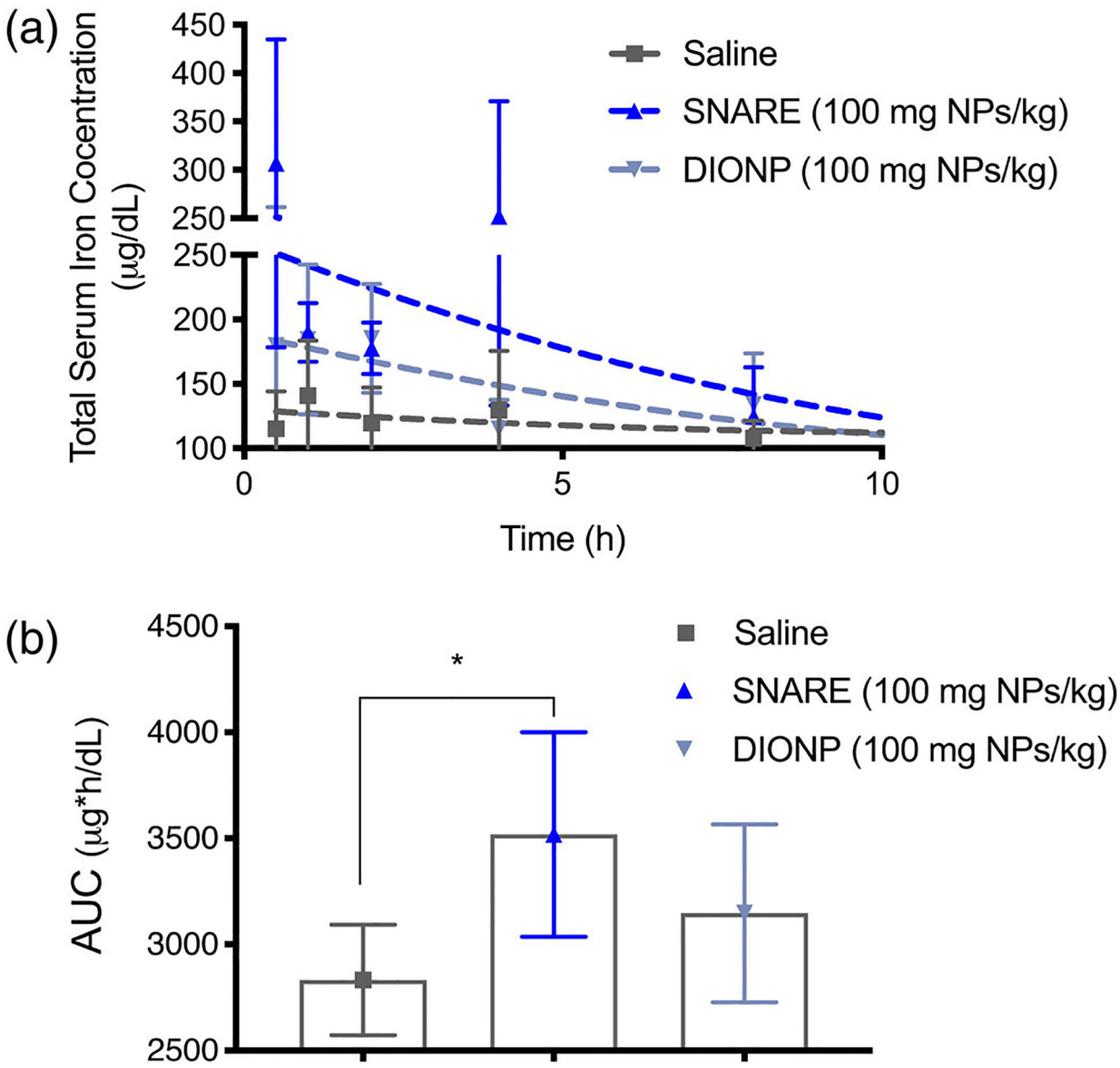

FIGURE 14.

Clearance of intravenously injected SNAREs in pregnant dams. Tail vein blood was collected at 30 min, 1, 2, 4, 8, 24 hr time points and total serum iron concentration determined (a). SNARE-treated dams demonstrated higher total serum iron concentration and thus slower clearance of NPs compared to DIONP-injected at earlier time points up to 8 hr postinjection. By 24 hr, total iron concentration for saline controls were similar to SNARE treated dams. (b) Area under the curve (AUC) demonstrated larger area and thus slower clearance of SNARE compared to DIONP